Visible and near-infrared multispectral analysis of rocks at Meridiani Planum, Mars, by the Mars Exploration Rover Opportunity

W. H. Farrand,[1] J. F. Bell III,[2] J. R. Johnson,[3] B. L. Jolliff,[4] A. H. Knoll,[5] S. M. McLennan,[6] S. W. Squyres,[2] W. M. Calvin,[7] J. P. Grotzinger,[8] R. V. Morris,[9] J. Soderblom,[2] S. D. Thompson,[7] W. A. Watters,[10] and A. S. Yen[11]

Received 12 June 2006; revised 13 September 2006; accepted 5 January 2007; published 26 April 2007.

[1] Multispectral measurements in the visible and near infrared of rocks at Meridiani Planum by the Mars Exploration Rover Opportunity's Pancam are described. The Pancam multispectral data show that the outcrops of the Burns formation consist of two main spectral units which in stretched 673, 535, 432 nm color composites appear buff- and purple-colored. These units are referred to as the HFS and LFS spectral units based on higher and lower values of 482 to 535 nm slope. Spectral characteristics are consistent with the LFS outcrop consisting of less oxidized, and the HFS outcrop consisting of more oxidized, iron-bearing minerals. The LFS surfaces are not as common and appear, primarily, at the distal ends of outcrop layers and on steep, more massive surfaces, locations that are subject to greater eolian erosion. Consequently, the HFS surfaces are interpreted as a weathering rind. Further inherent spectral differences between layers and between different outcrop map units, both untouched and patches abraded by the rover's Rock Abrasion Tool, are also described. Comparisons of the spectral parameters of the Meridiani outcrop with a set of laboratory reflectance measurements of Fe^{3+}–bearing minerals show that the field of outcrop measurements plots near the fields of hematite, ferrihydrite, poorly crystalline goethite, and schwertmannite. Rind and fracture fill materials, observed intermittently at outcrop exposures, are intermediate in their spectral character between both the HFS and LFS spectral classes and other, less oxidized, surface materials (basaltic sands, spherules, and cobbles).

Citation: Farrand, W. H., et al. (2007), Visible and near-infrared multispectral analysis of rocks at Meridiani Planum, Mars, by the Mars Exploration Rover Opportunity, *J. Geophys. Res.*, *112*, E06S02, doi:10.1029/2006JE002773.

1. Introduction

[2] In designing the Mars Exploration Rovers, a guiding principle was that the rovers would function as robotic field geologists. As such, the intent was to mimic, to the extent possible, the capabilities of a human presence in the field [*Squyres et al.*, 2003], including the ability to use a hand lens in order to view in close detail the textures of rock and soil, to scratch or chip a rock to reveal a fresh surface, and to assess rock and soil color. These capabilities were emulated on the rover, respectively, with the Microscopic Imager (MI), the Rock Abrasion Tool (RAT), and the Panoramic Camera (Pancam).

[3] The Mars Exploration Rover (MER) Opportunity landed on Meridiani Planum on 24 January 2004, fortuitously coming to rest in a 20 m diameter crater, later dubbed Eagle. Within the northern and western walls of Eagle crater lies a succession of layered bedrock, with approximately 30–50 cm of exposed strata. Description and interpretation of this outcrop are given by *Squyres et al.* [2004], *Bell et al.* [2004], *Christensen et al.* [2004], *Herkenhoff et al.* [2004], *Klingelhöfer et al.* [2004], *Rieder et al.* [2004], and *Grotzinger et al.* [2005].

[4] After 59 sols exploring the outcrop and soils of Eagle crater, Opportunity left its landing site and ventured eastward across the plains (Figure 1a). Outcrop exposures were observed at the Anatolia fracture system and at Fram crater,

[1] Space Science Institute, Boulder, Colorado, USA.
[2] Department of Astronomy, Cornell University, Ithaca, New York, USA.
[3] U.S. Geological Survey, Flagstaff, Arizona, USA.
[4] Department of Earth and Planetary Sciences, Washington University, St. Louis, Missouri, USA.
[5] Botanical Museum, Harvard University, Cambridge, Massachusetts, USA.
[6] Department of Geosciences, State University of New York, Stony Brook, New York, USA.
[7] Department of Geological Sciences, University of Nevada, Reno, Reno, Nevada, USA.
[8] Division of Geological and Planetary Sciences, California Institute of Technology, Pasadena, California, USA.
[9] NASA Johnson Space Center, Houston, Texas, USA.
[10] Department of Earth, Atmospheric and Planetary Sciences, Massachusetts Institute of Technology, Cambridge, Massachusetts, USA.
[11] Jet Propulsion Laboratory, California Institute of Technology, Pasadena, California, USA.

0148-0227/07/2006JE002773

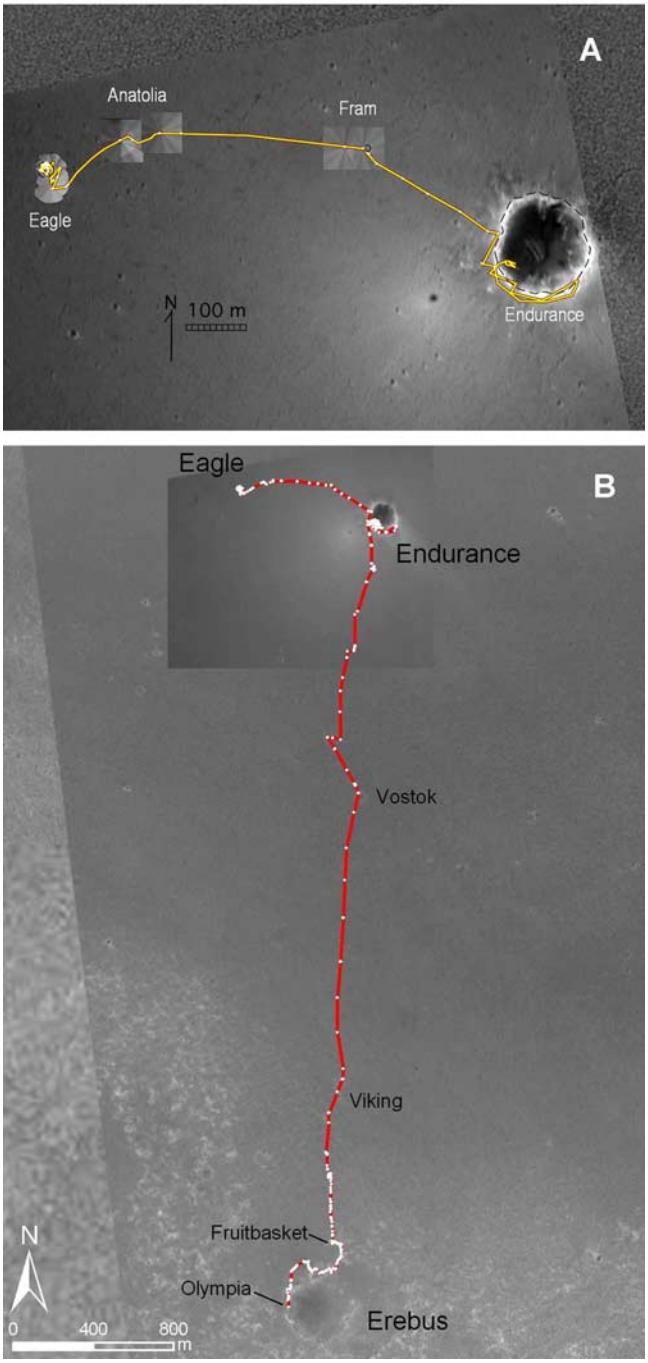

Figure 1. (a) Opportunity's traverse from Eagle to Endurance craters on a MOC base image. (b) Opportunity's complete traverse from Eagle crater to sol 741 and the Olympia outcrop at Erebus crater.

a smaller impact feature whose less degraded morphology suggests it is younger than Eagle. Approximately 7 m of exposed stratigraphic section were observed and studied along the inner wall of the 140 m diameter Endurance crater [e.g., *Grotzinger et al.*, 2005]. After 180 sols in Endurance, Opportunity began a southward trek across a surface characterized by extensive sheets of windblown sediments, locally forming small bedforms with amplitudes of up to several tens of cm, and wavelengths of a few meters. Lighttoned patches of outcrop are commonly exposed within the depressions between these bedforms, which are starved of sediment and therefore discontinuous. This drive has the long term goal of reaching the 800 m diameter Victoria crater (Figure 1b). On this southward trek, Opportunity has examined several outcrop exposures, notably a section dubbed the "Fruitbasket" region and an area of extensive outcrop on the rim of Erebus crater christened "Olympia." More details on Opportunity's explorations are provided in this special section by *Squyres et al.* [2006a].

[5] The rocks exposed at Eagle, Endurance, and Erebus craters, and all intervening exposures, belong to the Burns formation, an informal stratigraphic designation named in recognition of the late mineralogist Roger Burns [*Grotzinger et al.*, 2005]. The Burns formation consists of sandstones with clasts of mixed aluminosilicate and sulfate minerals formed from a basaltic precursor in an acidic weathering environment [*Squyres et al.*, 2004]. Minerals present include ferric oxide and Mg, Fe, and possibly Ca sulfates, including hematite and jarosite [*Klingelhöfer et al.*, 2004; *Christensen et al.*, 2004]. The stratigraphy of the Burns formation has been interpreted as a "wetting upward" succession from eolian sand dune through eolian sand sheet to a wet interdune facies [*Grotzinger et al.*, 2005]. The outcrop has also experienced episodes of groundwater diagenesis and later episodes that produced surficial rinds and fracture fill materials [*McLennan et al.*, 2005; A. H. Knoll et al., Late diagenetic veneers, rinds, and fracture fill at Meridiani Planum, Mars, manuscript in preparation, 2007 (hereinafter referred to as Knoll et al., manuscript in preparation, 2007)]. Outcrops at Eagle crater comprise the upper portion of this sequence, whereas outcrops at Endurance revealed the middle and lower parts of the sequence as well. Units of roughly the same or perhaps higher stratigraphic level as those at Eagle have been examined on Opportunity's southern traverse.

[6] In mapping these outcrops, the color information provided by Opportunity's Pancam played a critical role. Here, we discuss Pancam observations made through sol 735 of Opportunity's ongoing mission, characterizing the visible and near-infrared (VNIR) multispectral properties of in situ and various displaced rocks exposed at Meridiani Planum. We assess how these observations contribute to our understanding of the mineralogy and diagenetic history of outcrop materials. We also describe how the color imaging capabilities of the Opportunity rover's Pancam were used to select specific in situ sampling targets and to facilitate a standard practice of field geologists: stratigraphic mapping.

2. Data

[7] Detailed descriptions of the Pancam instrument and preflight calibration are given by *Bell et al.* [2003]. Information on the ongoing operation of Pancam and calibration of Pancam data is provided by *Bell et al.* [2006a]. In brief, the Pancam has two 1024 by 1024 charge-coupled devices (CCDs) with a 30 cm stereo separation and a 0.27 mrad per pixel spatial resolution. Pancam is mounted 1.5 m above the ground on a mast (the Pancam mast assembly, or PMA). Each camera has an eight-position filter wheel. One filter position (the L1 band) is a broad band unfiltered channel, used for albedo panoramas [*Bell et al.*, 2005] and low light/

Table 1. Pancam Band Names, Centers, and FWHM Widths

Band	Center, nm	FWHM Width, nm
L7	432	25
L6	482	27
L5	535	19
L4	601	17
L3	673	16
L2	753	20
R1	436	25
R2	754	19
R3	803	20
R4	864	17
R5	904	25
R6	934	24
R7	1009	28

nighttime imaging. There are also two neutral density filters (the L8 and R8 bands) for solar observations. This leaves 13 filters covering 11 unique VNIR wavelength intervals for multispectral geologic investigations with the near-UV to visible filters in the left eye and the visible to near-IR (NIR) filters in the right eye. Table 1 lists the left eye and right eye band names, centers, and Full Width at Half Maximum (FWHM) values of the 13 ''geology'' bands.

[8] Over the course of the MER mission, ''full spectral coverage'' by the Pancam has consisted of 13 filter observations using the channels listed in Table 1. The analyses reported in this paper use these 13 filter observations. Multispectral image sequences from the Pancam left eye and right eye cameras were analyzed separately to determine regions of interest (sets of pixels) representative of the map units, stratigraphic layers and spectrally unique materials discussed here. Custom software developed at Cornell University to analyze Pancam data was used for the extraction of combined eye spectra. Spectra from the regions of interest were combined from both eyes with pixels selected manually from common areas. The software scaled the spectra to match at the L2 and R2 channels (centered at 753 and 754 nm, respectively). Overlap between 432 nm and 436 nm bands was sufficiently consistent that for clarity we show only the 432 nm band in spectral plots. ''Error bars'' in the spectral plots shown here do not represent instrumental error, but instead represent the standard deviation of the mean for pixels averaged together to form the spectra.

[9] The Pancam was calibrated before launch as described by *Bell et al.* [2003, 2006a]. With the acquisition of each multispectral data set, a calibration target was also imaged close in time to the observation. The calibration target (described by *Bell et al.* [2003, 2006a]) has four color chips, multiple gray rings and a post that casts a shadow across the gray rings, allowing for estimation of both direct and diffuse illumination. Multispectral image data from the calibration target, in conjunction with prelaunch calibration information, were used to convert raw image data to calibrated radiance and then to radiance factor or I/F (where I is the measured radiance and πF is the incident solar irradiance). Accumulation of airfall dust on the calibration target over the course of the mission was compensated for through the use of a two-layer Hapke model along with the known photometric properties of the calibration target [*Bell et al.*, 2006a, *Sohl-Dickstein et al.*, 2005].

[10] The solar incidence angle was recorded for each scene and image analysis software was used to convert the data to relative reflectance (R*, defined as I/F divided by the cosine of the incidence angle [*Reid et al.*, 1999; *Bell et al.*, 2006a]). *Bell et al.* [2006a] estimated the absolute reflectance levels of these data to be accurate to within ~10% at the shortest wavelengths, and probably slightly less at longer wavelengths. Relative filter-to-filter uncertainties in R* were estimated to be typically 1–5%, providing confidence in the reality of even very small-scale spectral variations detected in a given scene. The 13-filter data sets examined here were typically compressed on the rover before downlink using a 12- to 8-bit square-root lookup table and a wavelet-based compression scheme so that blue stereo bands (the L7 and R1 bands) retained an effective compression rate of 2 bits-per-pixel (compression ratio of 6:1) and all other bands were at a rate of 1 bit-per-pixel (compression ratio of 12:1). Some of the scenes considered here had lesser amounts of compression, including some sequences that were losslessly compressed. The effects of these levels of compression on radiometric precision were estimated to be < 1% on the basis of prelaunch tests [*Bell et al.*, 2006a].

[11] Diffuse illumination from the Martian atmosphere provides a component of the incident illumination on the surfaces observed by Pancam. However, calibration of the images to R* results in a first-order correction of diffuse sky illumination for surfaces at or near the same solar incidence angle as the calibration target. *Johnson et al.* [2006] demonstrated that effects of diffuse illumination increase with incidence angle (i). Consequently, scenes were selected for use in the comparisons described below with i values that were approximately 25° or less in order to minimize the influence of skylight with increasing i. Although there are differences in magnitude of the diffuse illumination on a sol-by-sol basis, these differences are typically small compared to those on a seasonal basis, and are for the most part removed by the R* calibration process. This assertion is supported by the relatively smooth sol-to-sol variations in sky color measured by *Bell et al.* [2006b], even during the few periods of relatively high atmospheric dust opacity measured by Opportunity. Further, as will be shown below, comparisons of spectra from units with similar morphologic and textural features (i.e., those believed to be from the same stratigraphic unit compared over long distances and separated in time) can have spectral parameters that match better than those of surrounding units (see section 6.2).

3. Color Analysis and Spectral Parameterization Approach

[12] The most basic discrimination of color properties in Meridiani outcrop materials was made on the basis of simple three band color composites; most often using a default 2% stretch (i.e., excluding the highest and lowest 2% of R* values). Left eye composites frequently used the L2, L5, and L6 (753, 535, and 482 nm) or L3, L5, L7 (673, 535, and 432 nm) filters. Right eye composites were not as standardized, but a composite such as R5, R2, and R1 (904, 754, 436 nm) maximized right eye wavelength differences. Henceforth, a band combination such as the L3, L5, and L7 combination will be referred to as a L357 composite.

Table 2. Description of Spectral Parameters Used in This Study

Parameter	Description
R^*_{750}	R* value at 753 nm from the left eye
Red/blue ratio	L2/L7 (753 nm band/432 nm band)
482 to 535 nm slope	$(R^*_{535} - R^*_{482})/(535 - 482)$
535 nm spectral inflection	$[(0.570 \times R^*_{432}) + (0.430 \times R^*_{673})] - R^*_{535}$
601 nm spectral curvature	$[(0.522 \times R^*_{535}) + (0.478 \times R^*_{673})] - R^*_{601}$
535 to 601 nm slope	$(R^*_{601} - R^*_{535})/(601 - 535)$
904 nm relative band depth	$[(0.510 \times R^*_{800}) + (0.430 \times R^*_{1009})] - R^*_{904}$
754 to 1009 nm slope	$(R^*_{1009} - R^*_{754})/(1009 - 754)$
934 nm/1009 nm ratio	R6/R7 (934 nm band/1009 nm band)

[13] Color differences that are subtle in these simple three color composites were exaggerated through the use of a decorrelation stretch [*Gillespie et al.*, 1986] of the bands. The decorrelation stretch (DCS) consists of a principal components (PC) transformation of three selected image bands. The PC transformed bands are contrast stretched and then transformed back into the original image space. Through this transformation, subtle color differences become dramatically enhanced, allowing better discrimination among rock and soil types. The final result of the DCS depends on the materials, and accompanying spectra, contained in the scene. For this reason, DCS images shown in this paper, when compared to other DCS images, are calculated on the basis of portions of a scene with a similar set of spectral properties. For example, we compare near-field scenes with near-field scenes and far-field scenes with far-field scenes. Given that a consistent set of materials exist at sites examined to date by Opportunity on Meridiani Planum (e.g., sulfate-rich outcrop, basaltic sands, hematitic spherules, and occasional cobbles or bright drift) this type of comparison is deemed to be valid for comparing materials with similar colors in similar types of scene settings. We recognize the potential for illumination differences among image sets acquired at different times of day to produce viewing geometry variations that could complicate such comparisons. However, we minimize this possibility by using Pancam scenes acquired dominantly between ~10:00 Local True Solar Time (LTST) and ~15:00 LTST, for which spectral reflectance variations owing to photometric effects are minimized [*Johnson et al.*, 2006].

[14] In order to quantify color differences among outcrop units, a set of spectral parameters has been used. Many of these have been used in past studies of multispectral data sets collected on the Martian surface and via orbital or telescopic remote sensing [e.g., *McSween et al.*, 1999; *Bell et al.*, 2000; *Morris et al.*, 2002; *Farrand et al.*, 2006]. The spectral parameters reported in this paper were selected on the basis of their ability to highlight unique spectral differences between outcrop units in Eagle and Endurance craters; they are summarized in Table 2 and a discussion of the utility of the various parameters is provided next. We note that in the spectral parameter plots shown in this paper, we generally display several data points for each map/stratigraphic unit. Each point for a given unit represents a measurement of that unit from a distinct image sequence.

[15] The overall brightness, or albedo, of Meridiani Planum surface materials has been characterized in a number of albedo observations made using the L1 band of the Pancam over the course of the mission [*Bell et al.*, 2005]. The L1 has a 338 nm band pass and a band center at 739 nm. L1 observations were not made on many of the sections of outcrop considered here. Hence the R* value for the L2 band (753 nm) is used as a proxy for the L1 broadband albedo. The red/blue ratio and 535 to 601 nm spectral slope proved to be important discriminators of the degree of oxidation of outcrop materials. Also, as will be shown below, differences in the color of rock surfaces can be expressed well by 482 to 535 nm spectral slope differences. Another measure of the degree of crystallinity of ferric oxide minerals within the outcrop and/or their particle size is the degree of inflection in the spectral slope at the 535 nm band [e.g., *Morris et al.*, 1985] which we gauge by a relative band depth measure (Table 2). The curvature of the spectrum in the 600 nm region is related to the strength of the short wavelength ferric oxide absorption edge [e.g., *Sherman et al.*, 1982; *Morris et al.*, 1985] and is assessed here by a 601 nm curvature metric. Values for this metric tend to be negative with greater curvature leading to a more negative value.

[16] In the NIR or right eye channels, the 754 to 1009 nm spectral slope was extracted for scenes where the presence of red hematite was suspected. As is shown in Figure 2, a positive 754 to 1009 nm slope is indicative of the presence

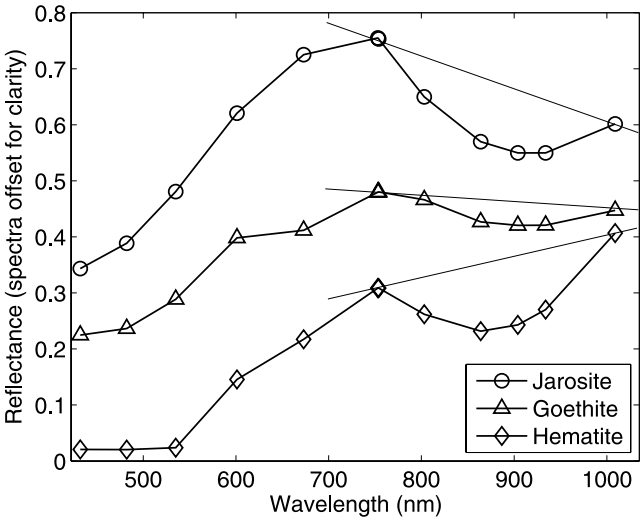

Figure 2. Illustration of the value of the 754 to 1009 nm slope parameter for distinguishing red hematite. Library spectra of hematite, goethite, and jarosite from the USGS spectral library [*Clark et al.*, 1993] are shown convolved to Pancam band passes, and lines are drawn through the 754 and 1009 nm band centers. Hematite has a positive 754 to 1009 nm slope; these samples of goethite and jarosite have negative slopes.

of red hematite. We note that the observation of a positive 754 to 1009 nm slope is not positive identification of the presence of red hematite, but is taken as a positive indication that it could be present. The R6/R7 ratio was useful for detecting the hematitic spherules that are ubiquitous on the Meridiani plains [e.g., *Bell et al.*, 2004]. A relative band depth metric, centered on the 904 nm band, is useful as a measure of the presence or absence of a long wavelength Fe^{2+}, Fe^{3+} or mixed ferrous and ferric iron crystal field band [*Burns*, 1993].

[17] Selection of regions of interest (ROIs) from which representative spectra, and associated spectral parameters, were extracted was accomplished through two approaches: image end-member regions identified through spectral mixture analysis and inspection of color and decorrelation stretch (DCS) composites. *Farrand et al.* [2006] describe how spectral mixture analysis (SMA) was applied to multispectral image sequences collected by the Pancam on the Spirit rover at Gusev crater. For a more thorough discussion of this methodology, see *Adams et al.* [1986, 1993]. In brief, SMA is an approach for modeling the measured spectrum of each image pixel as a linear combination of spectrally unique "end-member" spectra. "Image end-members" are single pixel or averages of pixel spectra extracted from the scene that represent the "purest" occurrences of the spectrally unique end-member materials. In practice, nonlinear effects may occur, but these effects are not so significant that they affect the selection of the end-member spectra. For example, a study [*Goetz and Kindel*, 1999] that utilized multiple data sets with different spatial resolutions did not detect additional end-members in the highest spatial resolution data (where nonlinear effects might be most pronounced). Also, as noted by *Tompkins et al.* [1997], nonlinear mixing results in curvature along the data clouds between end-members, not in the creation of new end-members. A standardized approach has been developed (included in the commercial ENVI software [*Research Systems, Inc.*, 2004]) for identifying at least an initial set of image end-members. Part of this end-member identification procedure involves the transformation of the data through a Minimum Noise Fraction (MNF) transformation [*Green et al.*, 1988], a transformation similar in nature to the principal components transformation [e.g., *Singh and Harrison*, 1985]. In some instances, spectrally unique materials were identified through direct study of the MNF bands. Materials whose spectral signature(s) depart significantly from what can be modeled through linear combination of the chosen image end-member spectra will show up as areas with high root mean square (RMS) error in an SMA modeled scene. For those scenes where outcrop and other surface materials could not be distinguished as separate end-member(s) via automated methods, representative areas on these materials had to be manually selected through reference to visual boundaries identified in the color composites and DCS images.

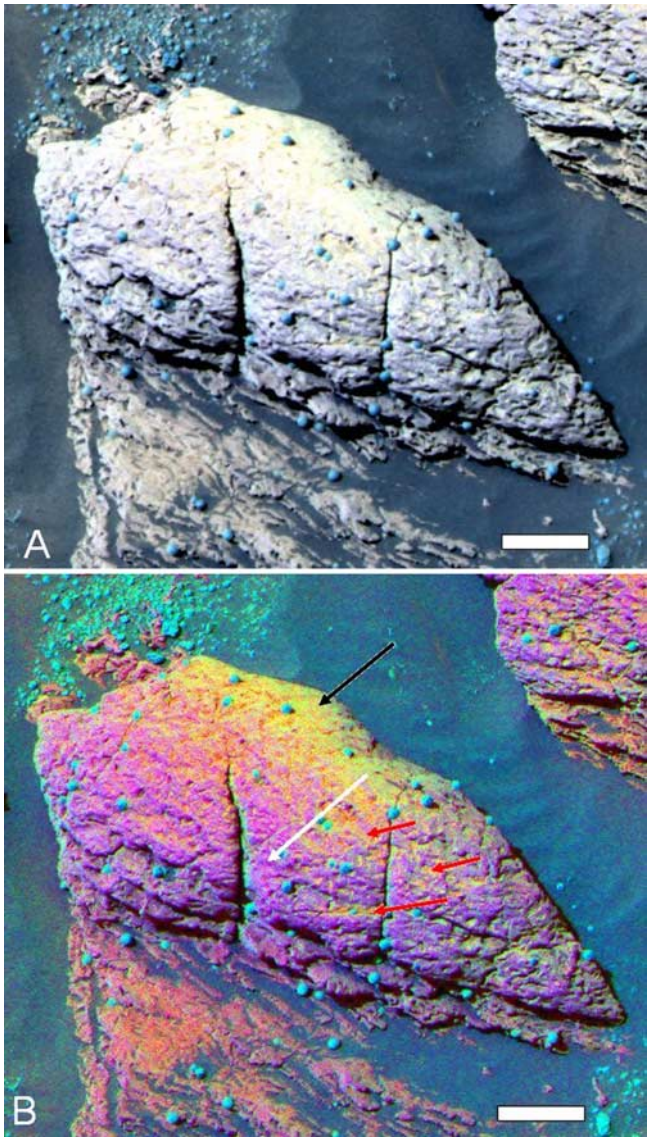

Figure 3. (a) Subsection of L357 color composite of the sol 38 image sequence P2538 viewing the rock Last Chance. Scale bar is 4 cm in length. (b) DCS version of this L357 composite. Black arrow points to an HFS class surface on outcrop. White arrow points to a LFS class surface. Red arrows point to furrows and vugs in the rock which are of the HFS spectral class.

4. Spectral Characterization of the Eagle, Endurance, and Southern Outcrop Exposures

4.1. Broad Color Classes and the Effects of Weathering

[18] In all occurrences of Burns formation outcrop observed by Opportunity, there are two basic spectral units into which all the observed stratigraphic units can be grouped. These spectral units appear in L357 composites as yellow to buff-colored and red to purple-colored outcrop (for example, see Figures 3–6). These color representations are made on the basis of the L357 composites and are more muted in "true color" representations of the Pancam color image sequences [e.g., *Savransky and Bell*, 2004; *Bell et al.*, 2006b]. A comparison of a true color representation compared with stretched versions is shown in Figure 5. In terms of their spectral parameters, the buff-colored surfaces have greater 482 to 535 nm slopes than do the purple-colored surfaces. For the purposes of labeling, these two color classes will be referred to in this paper as the "HFS"

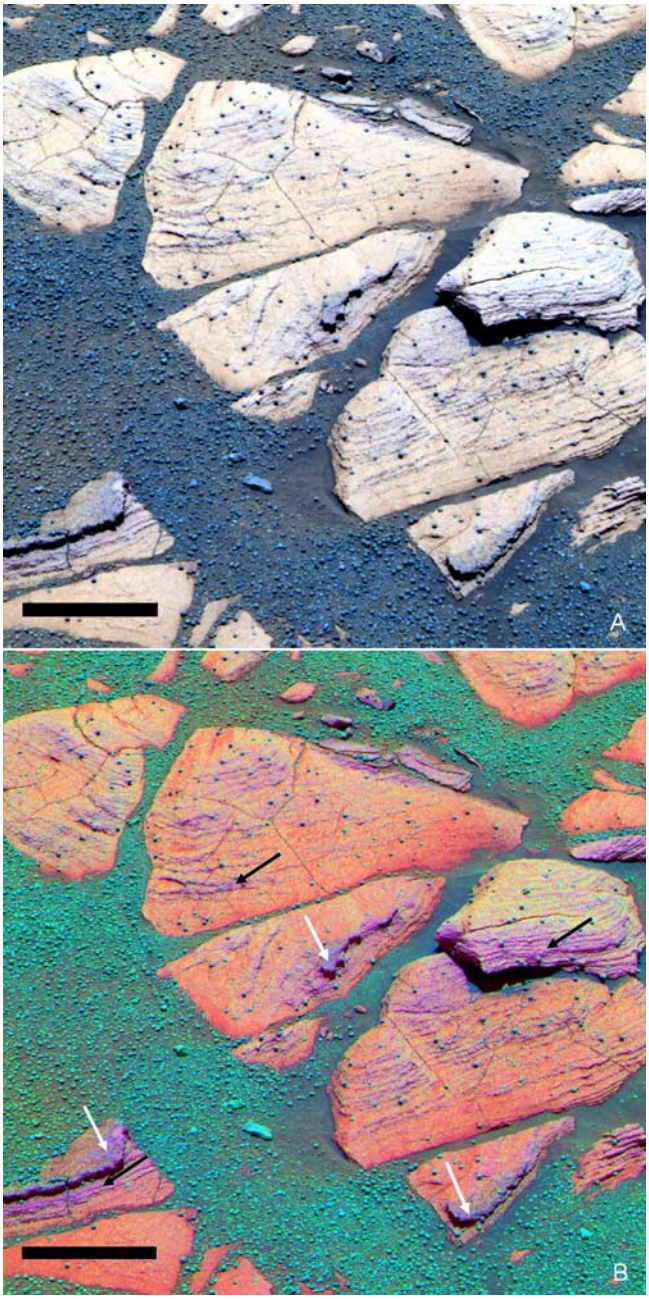

Figure 4. (a) Sol 50 P2575 L357 (673, 535, 432 nm) composite of unit A tabular rocks in the Shoemaker's Patio area. (b) DCS composite of the same band for the same scene. "Dark rind" and LFS surfaces on the outer borders of layers are indicated by white and black arrows, respectively. Scale bar in bottom left is approximately 11 cm in length.

(**H**igher **F**our hundred eighty-two to 535 nm **S**lope) and "LFS" (**L**ower **F**our hundred eighty-two to 535 nm **S**lope) spectral units. Some occurrences of the HFS outcrop surfaces have relatively high red/blue ratios and 535 to 601 nm slopes and are thus somewhat "redder." In contrast, some of the rind/fracture fill material (see section 4.6) can have higher reflectances at the shortest wavelengths and can be considered more "blue." Likewise, spherules and cobbles observed throughout the mission are more "blue" in appearance, with higher reflectances at the shortest wavelengths. While the main focus of this paper is on the spectral properties of rocks, for comparison purposes, Figure 7 shows representative spectra of all of the primary Meridiani Planum surface materials: HFS outcrop, LFS outcrop, spherules, and basalt sand as taken from the sol 33 P2589 scene shown in Figure 6 and the sol 38 P2538 scene shown in Figure 3.

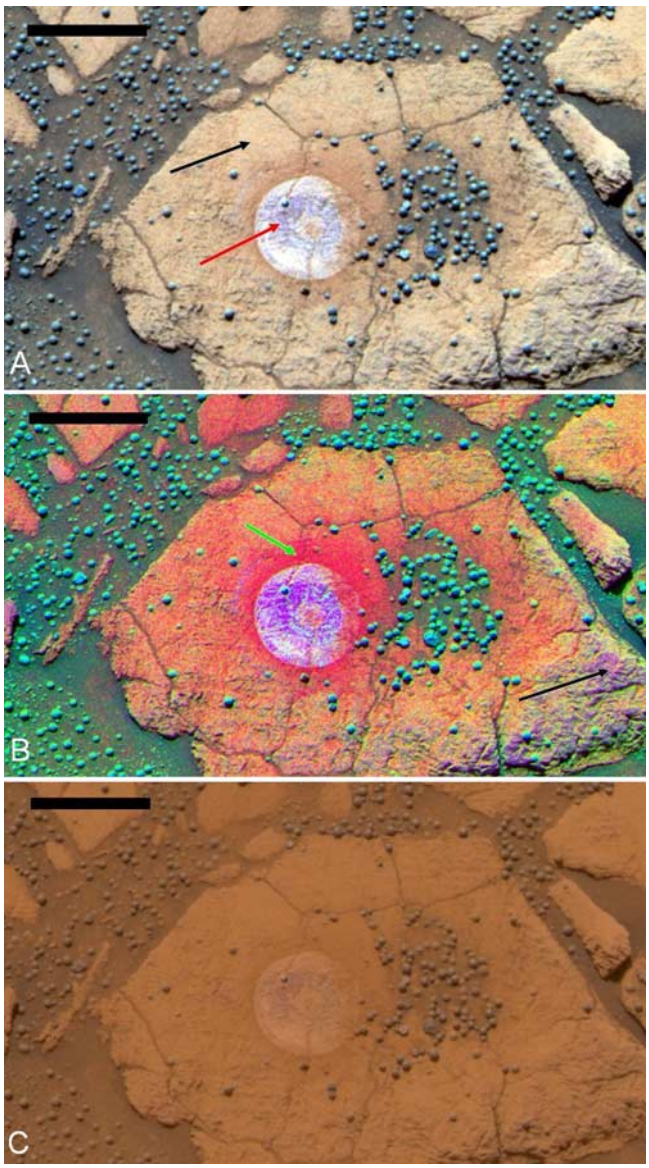

Figure 5. Sol 48 L357 view of the RAT brush spot on the rock Berry Bowl (Pancam sequence P2568). (a) L357 color composite. Red arrow marks purple LFS surface revealed by brushing as opposed to buff HFS weathered surface (marked by black arrow). Scale bar in each image is 5 cm in length. (b) DCS version of the L357 composite. Natural LFS surfaces (marked by black arrow) are observed on the steeper face of this rock. Also more apparent in this stretched image is the blanket of redder material (marked by green arrow) produced by the action of the RAT brush. (c) "True color" version of this scene.

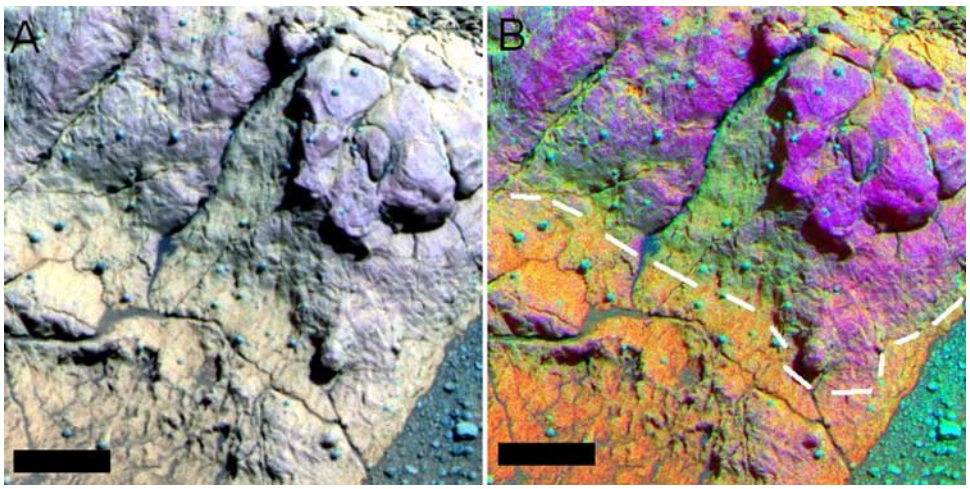

Figure 6. (a) L357 composite of a subsection of the sol 33 P2589 image sequence of the rock target "Cathedral Dome." Scale bar in bottom left is approximately 5 cm in length. (b) L357 DCS composite. Note the massive appearing purple-colored LFS subunit (top right) and the more tabular buff-colored HFS subunit (bottom left) separated by dashed white line.

[19] As described by other authors [e.g., *Squyres et al.*, 2004; *Grotzinger et al.*, 2005], outcrops are thinly laminated with the character of the bedding changing depending on position within the section. Certain portions of outcrop appear superficially to be massively bedded; however, the appearance of massive bedding has been interpreted as a consequence of diagenetic recrystallization [*McLennan et al.*, 2005] since relict laminations have been observed in "massively bedded" outcrop. Furthermore, areas that appear to be massive in normally incident light are often revealed to be laminated under conditions of low lighting angles [*Grotzinger et al.*, 2005]. The massive-appearing sections of outcrop, such as the El Capitan portion of the Eagle crater Opportunity Ledge outcrop, are always purple-colored in L357 composites. Thinly bedded sections of outcrop are lighter-toned, but can have layers that are darker-toned (Figure 8).

[20] One possible explanation for some portions of the outcrop having more HFS surfaces and other parts more LFS is that the HFS surfaces may be weathering rinds. This hypothesis is discussed in more detail by Knoll et al. (manuscript in preparation, 2007); however, some of the key supporting observations are presented here since they are directly relevant to understanding the multispectral VNIR color properties of the Meridiani outcrop. LFS surfaces are most often associated with steeper faces (such as the Cathedral Dome feature shown in Figure 6) and the distal portions of layers. HFS surfaces are most often flat-lying surfaces. For example, Figure 3 shows a L357 composite and a DCS version of the image sequence of the rock "Last Chance" in Eagle crater. The flat top of that rock is buff-colored (HFS spectral class) and the steeper face is purple-colored (LFS spectral class). Also of consequence, vugs and other furrows or cracks in the rock are buff-colored. One possible interpretation is that the steeper faces (which have been shown to be more resistant to RAT grinding [*Arvidson et al.*, 2004] and are thus presumably more resistant to erosion) are more subject to eolian stripping and thus the HFS material is a veneer that is being stripped away; however, that veneer remains on more flat-lying surfaces (area below dashed white line in Figure 6b) and in sheltered vugs and furrows (as at Last Chance in Figure 3b). This is also seen in the rocks exposed at the "Shoemaker's Patio" portion of the outcrop at Eagle crater shown in Figure 4. These rocks are generally tabular, but the exposed distal faces of the layers are more purple-colored. Another example is shown in Figure 5 where it is shown that the action of the RAT brush on the rock Berry Bowl stripped away a HFS veneer to leave a LFS surface.

[21] The distinction between HFS and LFS color units is the most obvious color difference among exposures of the Burns formation examined by Opportunity; however, as will be shown below, there are also color differences among surfaces abraded by the RAT and among individual layers

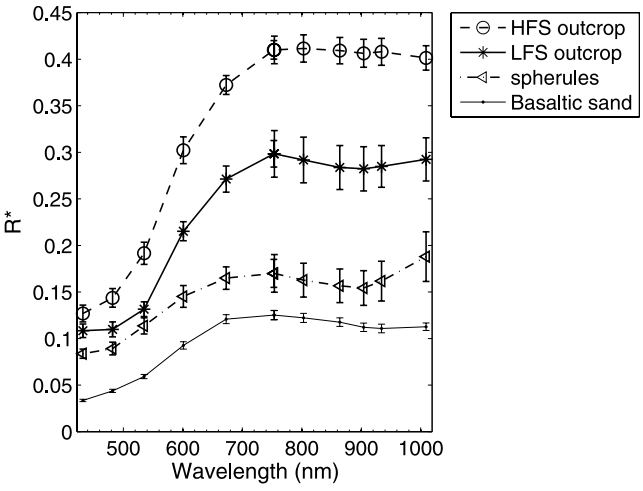

Figure 7. Representative spectra of Meridiani Planum surface units, all taken from the sol 33 P2589 scene shown in Figure 6 except for the basalt sand spectrum, which was taken from the sol 38 P2538 scene shown in Figure 3. Note that "error bars" in this and succeeding spectral plots represent the standard deviation of pixels averaged together to form average spectra and not instrumental error.

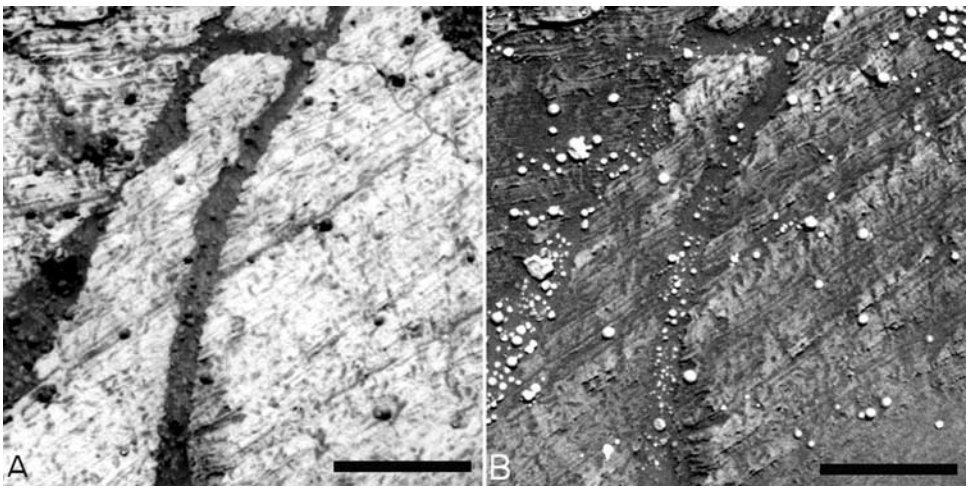

Figure 8. (a) L3 band (673 nm) of a subsection of the sol 42 P2547 image sequence on ''Slickrock,'' a representative of the Eagle B unit. (b) The second Minimum Noise Fraction (MNF) band derived from a MNF decomposition of the sol 42 P2547 left eye image sequence. Note alternating bright and dark layers in the MNF band, which are not apparent in the single band image. This is interpreted as inherent color differences between layers. Spherules are bright in this image also. Scale bar in the bottom left is 5 cm in length.

(Figure 8 and discussed also by *Thompson et al.* [2006]). We suggest that the bulk color properties of stratigraphic map units, such as will be described below from Eagle and Endurance craters, are dictated by the assemblage of layers present. That is, a greater fraction of darker-toned layers will lead to a darker-toned map unit. For example, the B map unit from Eagle crater shown in Figure 8 has a greater fraction of light-toned layers. Moreover, if we interpret the HFS surfaces as a weathering veneer, the properties of that veneer are a consequence of the properties of the underlying material. Below, we note that occurrences of the HFS and LFS spectral units in different map units have discernable spectral differences beyond just those shorter wavelength left eye differences discussed thus far. Thus the interpretation of the HFS surfaces as a weathering veneer does not mean that such surfaces cannot be used to help define stratigraphic correlations (as discussed in section 6).

[22] Rocks have also been observed which seem to lack any evidence of a HFS veneer. The rock ''Shark's Tooth,'' also from the Shoemaker's Patio region, provides a good example (Figure 9). Shark's Tooth is a displaced rock that might have been exposed by the impact that formed Eagle crater or it might be ejecta from a more distant impact. Another rock characterized as being within the LFS spectral unit, examined by Opportunity's in situ instruments on and around sol 105, is the rock ''Lion Stone'' on the outer rim of Endurance crater. The fact that some of the displaced rocks do not display the HFS veneer could have implications for the time of formation of the veneer. This will be discussed further in section 7.

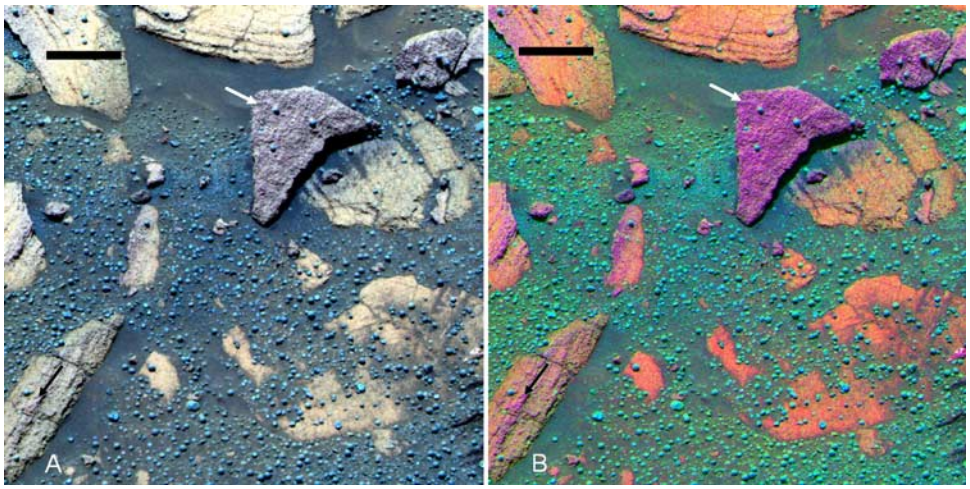

Figure 9. (a) Subsection of sol 51 P2584 L357 composite viewing Instrument Deployment Device (IDD) targets Shark's Tooth (white arrow) and Raspberry Newton (black arrow). Scale bar in the top left is 6 cm in length. (b) DCS composite of the same subsection and bands. Note that the black arrow points out a darker color layer in the rock Raspberry Newton.

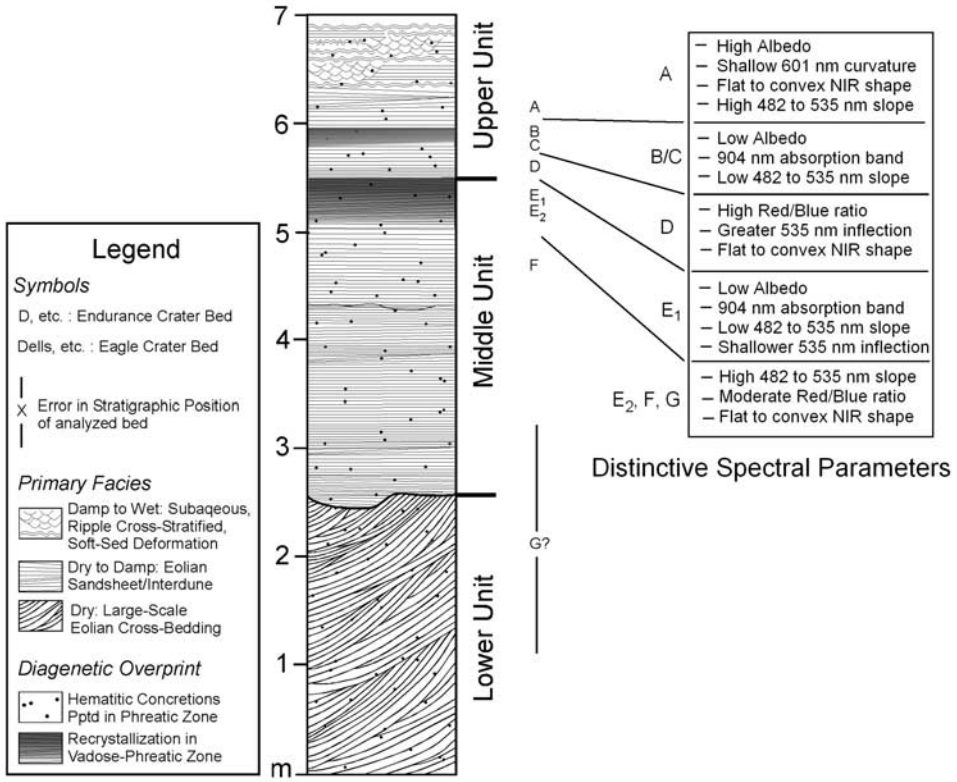

Figure 10. Burns formation stratigraphic column adapted from *Grotzinger et al.* [2005]. Distinctive spectral parameters of individual units and groups of units (with similar spectral characteristics) of the Karatepe ingress path are related to the stratigraphic units.

[23] Wherever Opportunity's RAT ground into outcrop, the cuttings from the RAT are visibly redder than the undisturbed outcrop (e.g., Figure 5b). This has generally been interpreted as the result of coarse gray hematite from spherules and disseminated gray hematite in the outcrop itself being comminuted by the RAT to finer-grained red hematite, producing the equivalent of a ''streak'' test commonly used as a simple mineralogical identification test. This observation supports the idea that there is a significant component of disseminated hematite in the outcrop in addition to the spherules, and that hematite in Meridiani is not restricted only to the spherules or so-called ''blueberries'' [e.g., *Bell et al.*, 2004; *Klingelhöfer et al.*, 2004]. Spectral parameters that might be associated with an increased fraction of red hematite are also observed, including an increase in the slope inflection at 535 nm and an increase in the 754 to 1009 nm slope.

4.2. Overview of the Physical Stratigraphy of the Burns Formation

[24] *Grotzinger et al.* [2005] presented a stratigraphic succession for the Burns formation based on observations made at Endurance and Eagle craters, which is adapted here as Figure 10. The lowermost beds observed constitute the Lower Unit and consist of large scale, cross-bedded sandstones interpreted as eolian dune deposits. This unit is truncated at the top by a deflation surface and is overlain by a Middle Unit characterized by planar stratified to low angle cross-stratified sandstones believed to represent an eolian sand sheet. The contact between the Lower and Middle Units in the type outcrop area of the Burns formation has been designated as the Wellington contact. The Middle Unit preserves evidence of episodically damp to wet environments. The upper part of the Middle Unit is a zone of recrystallization interpreted to have formed in the capillary fringe of the water table. The contact between the Middle and Upper Units has been called the Whatanga contact. Rock surfaces above and below the Whatanga contact are texturally very different, with Microscopic Imager images showing well defined, finely laminated bedding above the contact and a coarser, more nodular texture below [*McLennan et al.*, 2005; *Herkenhoff et al.*, 2006] (see Figure 11). The Upper Unit consists of both eolian sand sheet and subaqueous interdune facies, with the latter characterized by small scale festoon cross lamination and wavy bedding. The entire sequence is viewed as a ''wetting upward'' succession [*Grotzinger et al.*, 2005].

[25] The Lower Unit was well exposed at Burns Cliff in Endurance crater, but at the Karatepe ingress path was partially blanketed by basaltic sand and hematitic spherules. The Diamond Jenness, MacKenzie, and Inuvik RAT holes were ground into the Lower Unit, but the material in these RAT holes was friable and primary sedimentary structures were not well distinguished in these RAT holes. The Middle Unit was well exposed and subsequently examined at Endurance crater. The Upper Unit was identified in Endurance crater, and examined thoroughly at Eagle crater. Texturally similar outcrop has been recognized for some

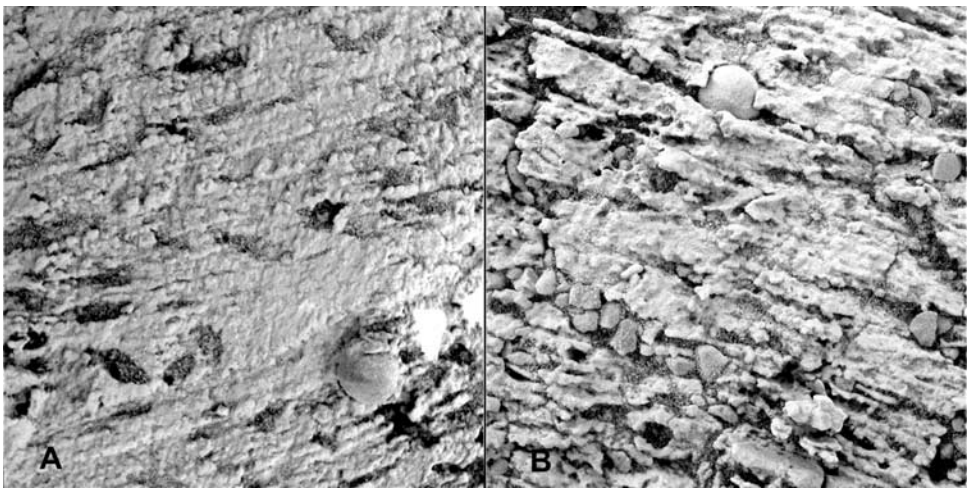

Figure 11. (a) Sol 148 MI pre-RAT image of the target London in Karatepe unit D. (b) Sol 151 MI pre-RAT image of the target Grindstone in Karatepe unit E1. Note the rougher texture in unit E1. In both of these images, the frame is approximately 31 mm across.

four kilometers (to date) along the path south from Endurance (e.g., at Vostok crater and at the Fruitbasket and Olympia outcrops near Erebus); at least some of this is likely to represent a stratigraphic level slightly higher than that recorded in the Endurance section. The component grains in the Middle and Upper units are rounded and uniform in size. They are cemented by Mg and, possibly, Ca sulfate minerals as well as the hydroxylated Fe sulfate, jarosite with the latter definitively identified on the basis of its Mössbauer signature [*Klingelhöfer et al.*, 2004]. The sulfate minerals likely originated via aqueous alteration of basalts in an acidic environment possibly within contemporaneous playas [*McLennan et al.*, 2005]. *McLennan et al.* [2005] also note that there is evidence for at least two and possibly more generations of cementing mineral phases in the outcrop.

[26] Color properties of these units are described below roughly in order of their examination by Opportunity. While the focus of this paper is on the color properties of the in situ Meridiani rock units, spectral parameters were also extracted from basaltic sands and hematitic spherules in order to compare color properties of the rocks against these materials. More detailed discussions of soils and spherules at Meridiani is provided by *Soderblom et al.* [2004] and *Weitz et al.* [2006]. A discussion of the relation of the color properties of the spherules and basaltic sands to outcrop is provided in section 5.3.

4.3. Eagle Crater

[27] The outcrop exposed in Eagle crater represents part of the Middle and Upper Units of the Burns formation as described above and by *Grotzinger et al.* [2005]. It was subdivided into five map units, A through E, according to color, morphology, texture and structural attitude [*Squyres et al.*, 2004]. Since lettered map units are also referenced for the Endurance crater Karatepe ingress route, these units are distinguished here, for example as ''Eagle unit A'' or ''Karatepe unit A.'' As noted above, the observed portions of outcrop all exhibited either HFS or LFS surfaces, but the relative proportion of these spectral units differed among map units as did their bedding characteristics (e.g., planar versus cross-bedded). In addition, there are more subtle spectral differences within these two broad color units which are discernable on the basis of some of the spectral parameters defined in Table 2. Measurements of these spectral parameters for representative surfaces from the Eagle crater units are plotted in Figures 13–15. To distinguish LFS from HFS surfaces, the former are plotted with open symbols and the latter with closed or cross symbols. Note especially the separability of these classes as illustrated by the separate LFS and HFS clusters in the 482 to 535 nm slope versus 904 nm relative band depth plot in Figure 13. Mean spectral parameter values for the Eagle crater units are summarized in Table 3. There were not a sufficient number of 13 filter observations of Eagle unit E for it to be included in this discussion.

4.3.1. Eagle Unit A

[28] Eagle Unit A is characterized by gently dipping beds, with planar lamination and low-angle stratification, which exhibit the HFS spectral signature on flat planar surfaces (Figure 4). Although Eagle unit A was not ground into by the RAT, at the Berry Bowl, this unit was brushed by the RAT, and the underlying color in the L357 composite of Figure 5 is consistent with that of LFS materials. Most of Eagle unit A is dominated by the HFS surfaces; however, the brushing at the Berry Bowl (Figure 5) and the presence of LFS surfaces at Shoemaker's Patio (discussed below) suggest that the HFS material might be a weathering veneer as mentioned above.

[29] Prominent exposures of Eagle unit A beds are found at the Shoemaker's Patio portion of the outcrop. Here, some rocks, especially on the distal ends of exposed layers and on some out-of-place blocks (such as the rock ''Shark's Tooth''), again could be characterized as LFS surfaces (Figure 4b, black arrows). There were also darker-toned red to purple-colored (in L357 DCS composites) rinds (Figure 4b, white arrows). One LFS rock examined with the Instrument Deployment Device (IDD) instruments was the rock Shark's Tooth (Figure 9). The tabular beds at

Table 3. Representative Spectral Parameters of Eagle Crater Stratigraphic Units and Other Materials[a]

Unit	R^*_{750} ($\times 10^{-1}$)	Red/Blue	482 to 535 Slope ($\times 10^{-4}$)	535 nm Inflection ($\times 10^{-2}$)	535 to 601 nm Slope ($\times 10^{-3}$)	601 nm Curvature ($\times 10^{-2}$)	904 nm Relative Band Depth ($\times 10^{-3}$)	754 to 1009 nm Slope ($\times 10^{-5}$)
A								
HFS	3.82 ± 0.08	4.90 ± 0.24	8.72 ± 0.71	4.12 ± 0.41	1.71 ± 0.096	−1.92 ± 0.57	5.20 ± 6.0	4.21 ± 2.9
LFS	2.82 ± 0.17	4.11 ± 0.25	4.92 ± 0.84	4.11 ± 0.45	1.36 ± 0.10	−1.51 ± 0.51	9.32 ± 5.0	−3.94 ± 2.8
Rinds	2.64 ± 0.13	3.42 ± 0.26	5.72 ± 0.92	3.01 ± 0.50	1.12 ± 0.49	−1.19 ± 0.50	9.49 ± 3.9	0.25 ± 2.9
B								
HFS	3.61 ± 0.074	5.00 ± 0.18	7.62 ± 0.55	4.49 ± 0.32	1.67 ± 0.070	−1.81 ± 0.48	5.86 ± 5.8	1.70 ± 2.7
RAT interior	3.73 ± 0.081	3.95 ± 0.15	6.48 ± 0.68	4.93 ± 0.40	1.83 ± 0.084	−2.96 ± 0.59	17.8 ± 5.5	3.40 ± 3.0
RAT cuttings	3.45 ± 0.13	6.41 ± 0.25	0.542 ± 0.50	5.98 ± 0.30	1.74 ± 0.094	−1.89 ± 0.39	19.7 ± 5.6	12.6 ± 3.3
C								
HFS	3.72 ± 0.081	4.34 ± 0.23	7.39 ± 0.81	3.84 ± 0.43	1.62 ± 0.22	−2.02 ± 0.54	7.34 ± 5.6	0.528 ± 3.2
LFS	2.84 ± 0.19	3.50 ± 0.24	3.75 ± 0.93	4.57 ± 0.43	1.37 ± 0.096	−1.47 ± 0.46	14.4 ± 4.6	−3.43 ± 3.1
RAT interior (Guadalupe)	2.22 ± 0.16	4.46 ± 0.39	2.16 ± 0.57	4.42 ± 0.29	0.87 ± 0.074	0.182 ± 0.27	16.4 ± 3.7	10.9 ± 2.8
RAT interior (McKittrick)	3.47 ± 0.12	4.67 ± 0.34	6.19 ± 0.71	5.46 ± 0.35	1.74 ± 0.079	−2.11 ± 0.37	17.5 ± 3.8	3.30 ± 2.8
RAT cuttings (Guadalupe)	3.95 ± 0.22	6.58 ± 0.62	5.09 ± 0.92	6.33 ± 0.50	1.76 ± 0.13	−0.787 ± 0.47	18.6 ± 3.6	19.6 ± 4.7
D								
HFS	3.30 ± 0.08	4.95 ± 0.25	9.92 ± 0.87	4.05 ± 0.49	1.92 ± 0.098	−2.57 ± 0.66	6.60 ± 6.9	0.070 ± 3.8
LFS	2.75 ± 0.16	3.41 ± 0.32	4.40 ± 1.5	3.20 ± 0.60	1.23 ± 0.15	−1.57 ± 0.80	10.5 ± 5.5	−4.28 ± 3.42
Spherules		1.42 ± 0.21	1.00 ± 2.8	0.01 ± 0.028	0.307 ± 0.15	−0.251 ± 0.71	16.5 ± 6.8	5.19 ± 4.6
Basalt sands		3.14 ± 0.17	2.26 ± 0.37	0.0226 ± 0.0037	0.469 ± 0.042	−0.410 ± 0.21	7.42 ± 2.7	−5.00 ± 1.9

[a]Values are averages, accompanied by standard deviation of the mean, of measurements from several patches on rock surfaces.

Shoemaker's Patio have variable dips that range from 0–15°.

[30] There was a discernable broader wave pattern on these beds, characteristic of the wavy bedding of the Burns formation Upper Unit noted above. The two in situ observations made at Shoemaker's Patio, Shark's Tooth and Raspberry Newton, appeared to be of out-of-place, or rotated, blocks. Layers in Raspberry Newton appeared to be oriented nearly perpendicular to the ground surface. A layer in Raspberry Newton appears redder than surrounding layers in the L357 DCS stretch (Figure 9b, black arrow). Shark's Tooth and Raspberry Newton both have elevated Cl relative to the RAT holes examined at Eagle and upper Endurance crater. Spectra of the LFS surfaces and the rinds in unit A (Figure 12) display shallower inflections at 535 nm than do the HFS surfaces. However, they have deeper 904 nm relative band depths than the HFS faces (accentuated in the continuum-removed right eye spectra in Figure 12b) and also have lower 482 to 535 nm slopes (Figure 13). Along with Eagle units B and D, the HFS surfaces of Eagle unit A have the highest red/blue ratios for Eagle crater units (Figure 14).

4.3.2. Eagle Unit B

[31] Unit B consists of thinly laminated outcrop and includes the rocks "Slickrock" and "the Dells" which both contain planar to low-angle stratification, festoon ripple cross-lamination, and crinkly to undulatory lamination [*Grotzinger et al.*, 2005]. Dips are steep in this unit, ranging up to 60°. The Slickrock exposure has layers varying in albedo and color and, as such, is a good example of inherent color differences between outcrop layers. Figure 8a shows the L3 image from the sol 42 P2547 sequence viewing Slickrock. Figure 8b shows the second MNF band derived from a MNF decomposition of this P2547 left eye image sequence. Tonal differences between layers are not pronounced in the single band image in Figure 8a; however, multispectral differences are amalgamated in the MNF transformation and thus are apparent in the MNF band shown in Figure 8b. There are layers with lower R^*_{750} values and lower 482 to 535 nm slopes as well as layers with higher R^*_{750} values and higher 482 to 535 nm slopes. Overall, Eagle unit B is dominated by brighter, HFS surfaces; hence Table 3 and the spectral parameter plots of Figures 13–15 report on only HFS surfaces from Eagle unit B.

4.3.3. Eagle Unit C

[32] Eagle unit C consists of a finely laminated subunit (examined in situ at the McKittrick RAT hole) and a recrystallized subunit. The latter subunit is also finely laminated; however, recrystallization has created a massive appearance (examined in situ at the Guadalupe RAT hole). These subunits are well expressed in the RAT holes located at the portion of the outcrop dubbed "El Capitan." The massive faces tend to display colors more representative of the LFS unit in L357 DCS composite images and the tabular beds display a lighter-toned exterior with HFS spectral characteristics. An example is shown in Figure 6 for a portion of the outcrop at the western end of the El Capitan region named "Cathedral Dome." Spectra of the different color units at El Capitan are shown in Figure 16a. Some of the LFS surfaces of Eagle unit C have the greatest inflections at 535 nm and deepest 904 nm absorption bands of any of the natural rock surfaces examined in Eagle crater (Figures 13 and 14).

[33] The spectrum of the RAT hole interior at Guadalupe appears to be heavily influenced by red hematite. The spectrum of the Guadalupe RAT cuttings appears to be even more highly influenced by red hematite (with a strong 535 nm spectral inflection and a long wavelength band minimum at 864 nm) (Figure 16a). In contrast, the spectrum

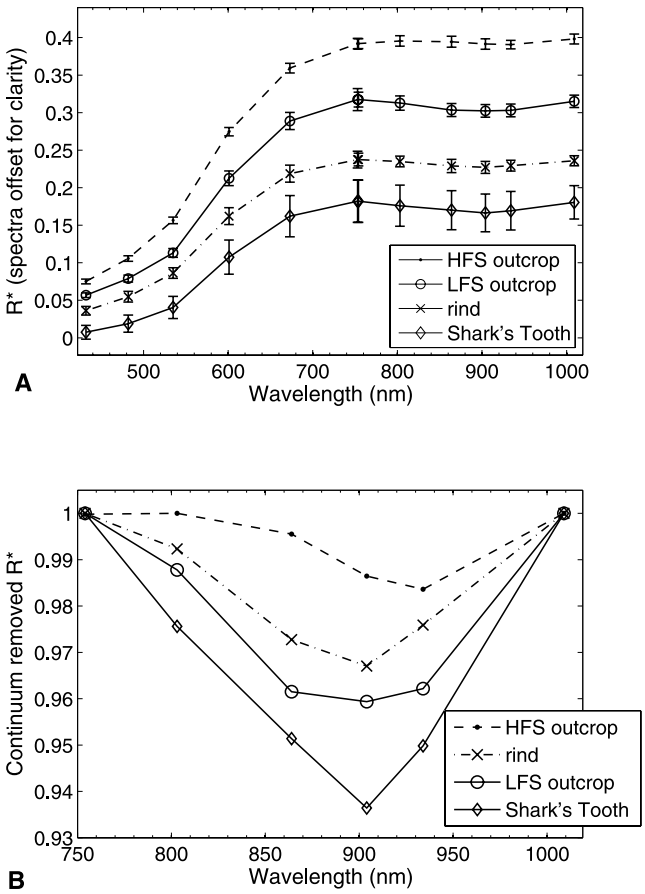

Figure 12. (a) Spectra of color units from within Eagle unit A. Note the relatively flat NIR reflectance of the HFS surfaces (top spectrum) and the shallower 904 nm band depth of the "rind" material compared to the LFS surfaces. The LFS spectrum has been offset downward by 0.02; the "rind" spectrum has been offset downward by 0.05. (b) Continuum-removed right eye spectra of these same observations, error bars removed for clarity.

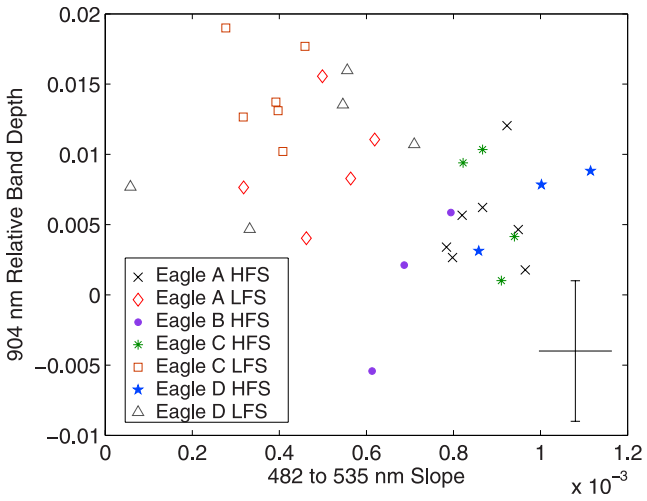

Figure 13. The 482 to 535 nm slope versus 904 nm relative band depth for Eagle crater units. Open symbols represent LFS surfaces; closed and cross symbols represent HFS surfaces. Representative error bars with average standard deviation values from units A and C are presented in the bottom right. Note that in this and succeeding spectral parameter plots, each point represents a measurement from an image sequence (i.e., for each map unit, multiple measurements from multiple image sequences are represented).

of the McKittrick RAT-hole interior (Figure 16b) has a higher albedo (indicated in Table 3 by the higher R^*_{750} value and by overall greater R* values in Figure 16b) and a lower 754 to 1009 nm slope indicative of less influence from red hematite. In these two RAT hole interiors, three spherules were partially ground into within the Guadalupe RAT hole and two within the McKittrick RAT hole. The grinding of one more spherule within Guadalupe versus McKittrick is not considered here to be the cause of the greater red hematite spectral characteristics of the hole interior, because MI images of the two RAT-hole interiors showed them to be relatively free of RAT cuttings. Also, if either of the two holes were to have a greater accumulation of fine dust (smaller than MI resolution), it would probably be McKittrick since it was nearly flat lying whereas Guadalupe was on a nearly vertical face. It can also be noted, on the basis of RAT grind time and grind depth, that Guadalupe was the hardest portion of outcrop examined during Opportunity's primary mission and McKittrick was one of the softest [*Arvidson et al.*, 2004]. This difference in hardness, in association with the evidence from Pancam of red hematite in the Guadalupe RAT-hole interior and in the associated RAT cuttings, suggests some difference in the mineralogy of these two portions of Eagle unit C. Mössbauer spectrometer results support this inference since the undisturbed Guadalupe surface had the highest hematite

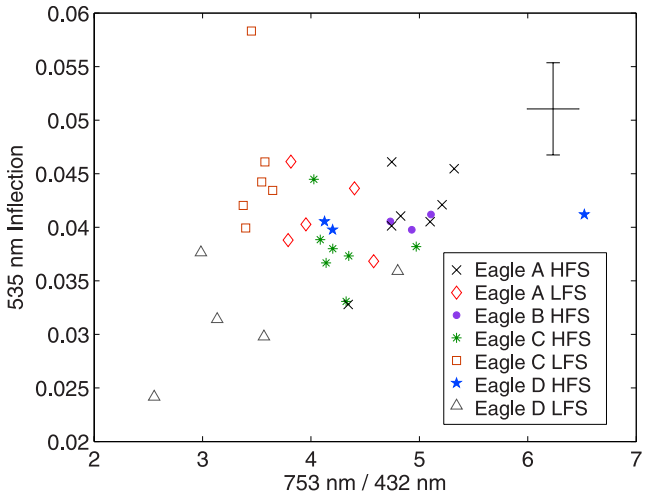

Figure 14. Red/blue (753 nm/432 nm) ratio versus 535 nm inflection for Eagle crater units. Open symbols represent LFS surfaces; closed and cross symbols represent HFS surfaces. Representative error bars with average standard deviation values from units A and C are presented in the top right.

Table 4. Representative Spectral Parameters of Undisturbed, Clean Surfaces of Endurance Crater Stratigraphic Units in the Karatepe Ingress Section[a]

Unit	R^*_{750}	Red/Blue	482 to 535 nm Slope ($\times 10^{-4}$)	535 nm Inflection ($\times 10^{-2}$)	535 to 601 nm Slope ($\times 10^{-3}$)	601 nm Curvature ($\times 10^{-2}$)	904 nm Relative Band Depth ($\times 10^{-3}$)	754 to 1009 nm Slope ($\times 10^{-5}$)
A	0.333 ± 0.009	7.72 ± 0.33	9.64 ± 0.59	4.13 ± 0.36	1.85 ± 0.084	−2.55 ± 0.56	−4.30 ± 4.9	−2.90 ± 2.6
B	0.235 ± 0.019	6.47 ± 0.41	6.52 ± 0.81	2.86 ± 0.39	1.23 ± 0.12	−1.66 ± 0.46	1.89 ± 4.1	−6.70 ± 2.6
C	0.251 ± 0.015	7.09 ± 0.38	6.89 ± 0.75	3.08 ± 0.38	1.28 ± 0.12	−1.60 ± 0.45	0.671 ± 3.9	−4.20 ± 2.5
D	0.304 ± 0.014	8.32 ± 0.34	7.85 ± 0.55	3.85 ± 0.29	1.52 ± 0.087	−1.66 ± 0.43	−3.9 ± 4.3	1.10 ± 2.8
E1	0.171 ± 0.022	6.20 ± 0.61	4.88 ± 1.0	2.12 ± 0.41	0.906 ± 0.13	−1.16 ± 0.44	1.36 ± 4.2	−3.70 ± 3.2
E2	0.288 ± 0.012	7.77 ± 0.38	8.40 ± 0.73	3.42 ± 0.33	1.50 ± 0.091	−1.95 ± 0.46	−4.12 ± 4.7	−4.20 ± 2.8
F	0.267 ± 0.013	7.72 ± 0.40	7.55 ± 0.68	3.36 ± 0.34	1.37 ± 0.086	−1.57 ± 0.41	−2.36 ± 3.8	−3.60 ± 2.4
G	0.282 ± 0.010	6.92 ± 0.31	8.16 ± 0.42	3.35 ± 0.31	1.48 ± 0.08	−1.95 ± 0.38	−2.69 ± 5.7	−8.20 ± 3.4

[a]Values are average values from within individual scenes accompanied by standard deviation of the mean.

abundance (45% of the iron in hematite [*Klingelhöfer et al.*, 2004]) of any of the in situ outcrop locations examined during Opportunity's primary mission.

4.3.4. Eagle Unit D

[34] Unit D includes the eastern part of the outcrop, called "Big Bend." Facies are dominated by crinkly bedding and small scale cross-lamination. The rock "Last Chance" is exposed here, which contains the festoon cross-lamination documented by *Squyres et al.* [2004] and *Grotzinger et al.* [2005]. In terms of color properties, unit D is also similar to unit C. Although this unit was not ground into by the RAT, the colors of the sections with the massive appearance are more like the LFS color unit. The brighter, HFS-like portions on top of these massively bedded areas appear to be a veneer as discussed above in section 4.1 and as illustrated in Figure 3. The darker-toned Eagle unit D LFS surfaces have the lowest red/blue ratios and shallowest 535 nm spectral inflections (Figure 14) and among the least negative 601 nm spectral curvatures (Figure 15) of the Eagle crater stratigraphic units. The lighter-toned HFS surfaces also had the highest 535 to 601 nm slopes (Figure 15).

4.4. Endurance Crater

4.4.1. Karatepe Ingress Stratigraphy

[35] Stratigraphy in Endurance crater was analyzed with the rover's IDD instruments along an ingress path at the "Karatepe West" region on the southwest rim of the crater, at points deeper within the crater (on blocks that were in some cases rotated or perhaps out-of-place), near the western portion of the "Burns Cliff" part of the south inner crater wall, and at the "Karatepe East" region where the rover exited the crater. A stratigraphic section of units A through G (with A being stratigraphically highest) was established along the Karatepe ingress path and are shown schematically in Figure 10 and in image format in the "Backroads" observation from sol 173 (Figure 17). These units were defined on the basis of their distinctive color and textural characteristics. Spectral characteristics of the most distinctive of these units (or groupings of these units) are summarized also in Figure 10. To avoid confusion with the units A – E established in Eagle crater, further discussion refers to those units as, for example, "Karatepe unit A." The exact relationship of the uppermost of the examined Endurance crater units to those examined at Eagle crater cannot be determined, but the uppermost examined unit (Karatepe unit A) is dominated by low angle cross-stratification, apparently lacking in festoon bedforms. Thus, in the stratigraphic framework established by *Grotzinger et al.* [2005], this would be consistent with it being stratigraphically below those beds at Eagle crater that display festoon bedforms.

[36] Upon its arrival at the rim of Endurance crater, Opportunity collected a set of panoramic and 13-filter views of the crater walls from the "pan position 1" site over sols 95 to 98. These views included a subframe 13-filter view of the Karatepe, and the more distant, Burns Cliff regions. R521 (903, 754, 436 nm) DCS composites taken from the pan positions on the rim showed distinct color differences between the upper and middle-to-lower units. This is illustrated in Figure 18 with R521 DCS composites of the Karatepe and Burns Cliff regions. Additional panoramic views were collected over sols 116 to 120 from the south rim of the crater at the "pan position 2" site.

4.4.2. Discussion of Spectral Properties of Karatepe Stratigraphic Units

[37] Representative spectra of the Karatepe ingress units are shown in Figure 19. Spectral parameters of the lettered Karatepe units are summarized in Table 4. Differences in the VNIR color properties of the Karatepe stratigraphic units are subtle but are discernable both through examination of spectral parameters and in three-color decorrelation

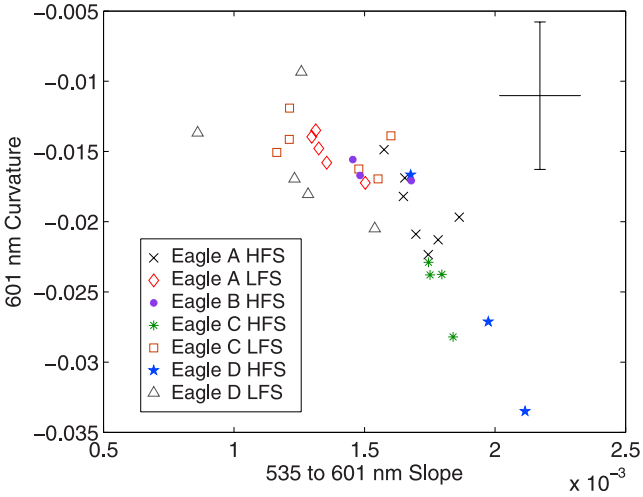

Figure 15. Plot of 601 nm curvature versus 535 to 601 nm slope for Eagle crater units. Open symbols represent LFS surfaces; closed and cross symbols represent HFS surfaces. Representative error bars with average standard deviation values from units A and C are presented in the top right.

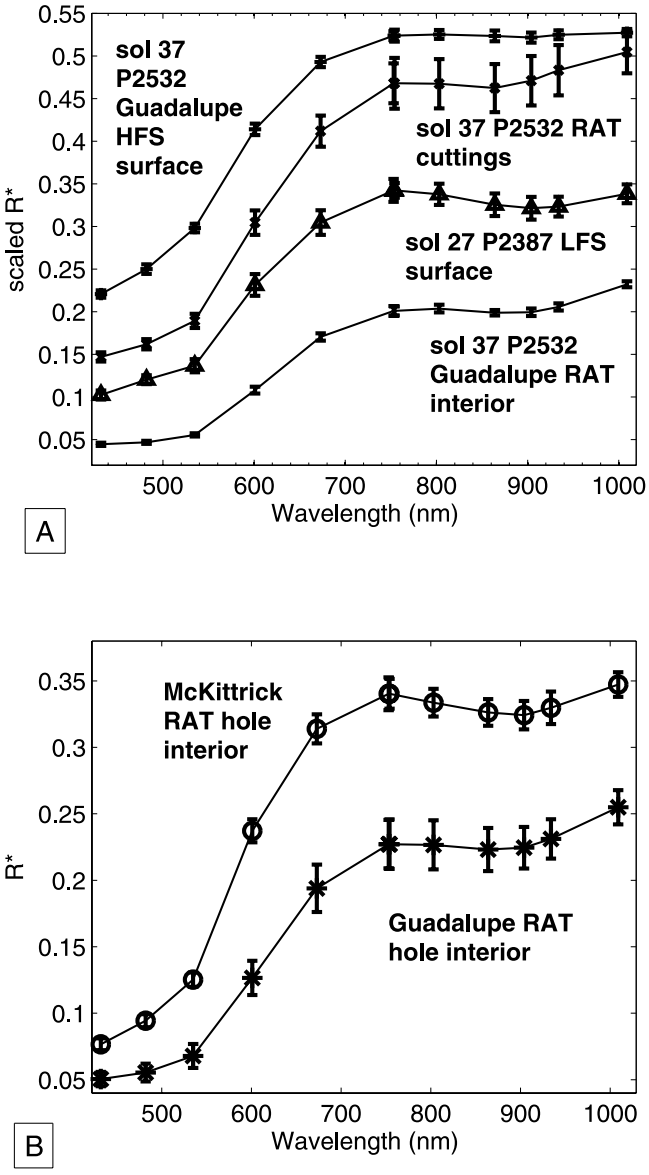

Figure 16. (a) Spectral units associated with the "Guadalupe" portion of the Eagle Crater "El Capitan" region. HFS spectrum has been offset upward by 0.13; RAT-cuttings spectrum has been offset upward by 0.09. (b) Comparison of spectra of RAT-hole interiors of Guadalupe and McKittrick. R* values have not been offset.

stretch images such as Figure 18. In terms of the spectra and the spectral parameters, the units differ in their R^*_{750} values and their 482 to 535 nm and 535 to 601 nm slopes. In the right eye bands, there are differences in whether the NIR spectrum is convex or concave. Spectra of the clean, RATted outcrop differ from the undisturbed surfaces and are shown in Figure 20 and spectral parameters for the RAT-hole interiors are presented in Table 5. Spectral parameter plots for the undisturbed Karatepe ingress units are shown in Figures 21–23. The greatest spectral differences are between light-toned units (e.g., A and D) and darker-toned units (e.g., B/C and E1) interpreted to have been subjected to diagenetic recrystallization [*McLennan et al.*, 2005]. To highlight these differences, the former units are represented in the spectral parameter plots by solid or star symbols and the latter units by open symbols.

4.4.2.1. Karatepe Unit A

[38] Unit A has the highest R^*_{750} of any Karatepe stratigraphic unit and, after unit D, the second highest red/blue ratio. Unit A also has the highest 535 to 601 nm slopes and have the greatest curvatures at 601 (Figure 21). Undisturbed surfaces have a convex NIR spectrum, but the "Tennessee" RAT hole interior has an absorption band centered at 904 nm (Table 5). The RAT hole interior also has a lower 482 to 535 nm slope.

4.4.2.2. Karatepe Units B and C

[39] While there are discernable spectral and chemical [*Clark et al.*, 2005] differences between the B and C units, they do plot together closely in the spectral parameter plots of Figures 21–23 and, so, are considered together here.

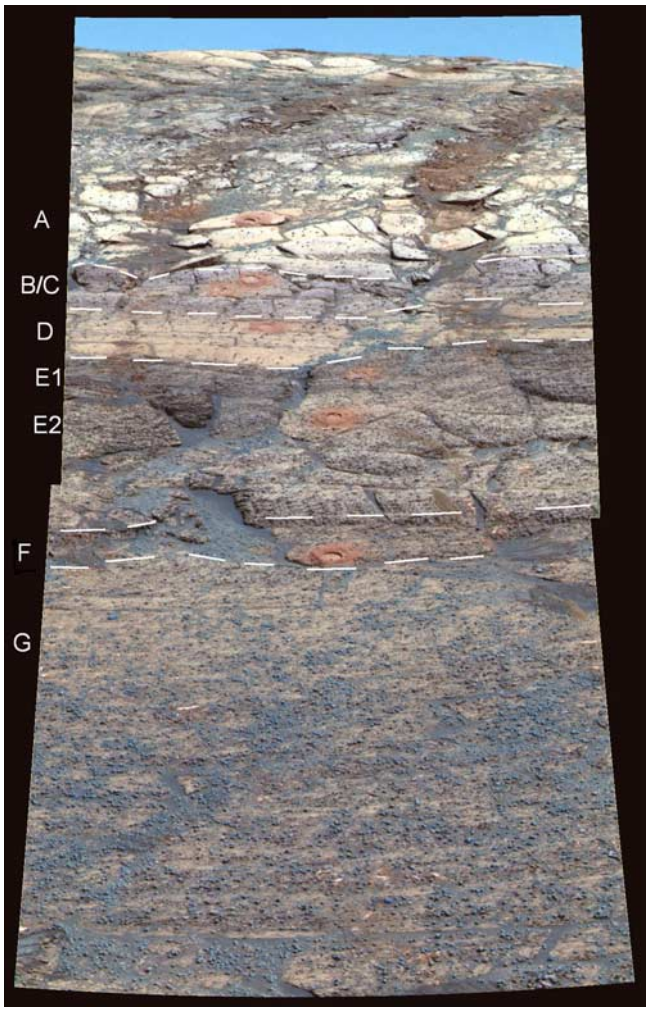

Figure 17. L357 composite and mosaic of the P2401 image sequence from sol 173. Karatepe stratigraphic units are annotated. RAT holes associated with each unit are as follows: A, Tennessee; B, Cobble Hill; C, Virginia; D, London; E1, Grindstone; E2, Kettlestone; F, Millstone. Scale can be assessed from diameters of the RAT holes (each is 4.5 cm in diameter) and the width of rover wheel tracks (the rover wheel is 16 cm in width).

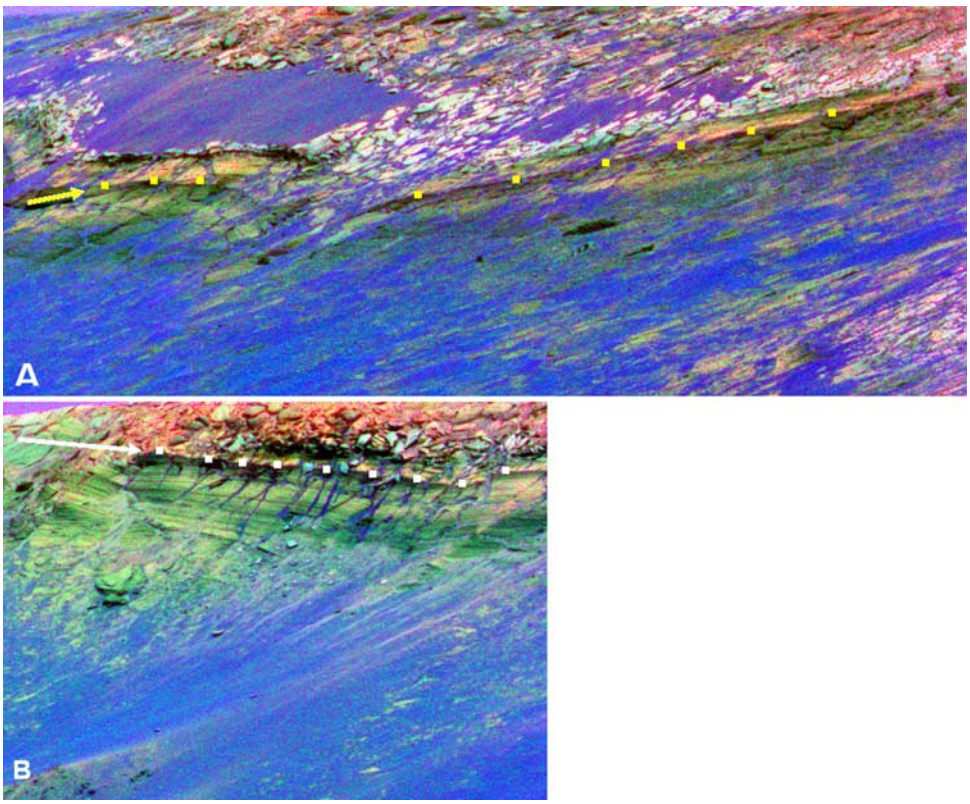

Figure 18. (a) DCS composite of R521 (904, 754, 436 nm) bands from sol 98 P2350 image sequence viewing the Karatepe region from pan position 1. Yellow arrow and string of yellow dots indicate the "Whatanga contact." The "Lower Unit" (E – G) appears green in this composite; rocks in the "Middle Unit" (D) are yellow-orange in this composite. (b) DCS composite of R521 bands from sol 97 P2559 image sequence viewing the Burns Cliff outcrop from pan position 1. White arrow and string of white dots indicate the Whatanga contact.

Along with unit E1, unit B has a concave NIR spectrum and a low 482 to 535 nm slope (Figure 22) and is lower in R^*_{750} than other Karatepe units (Table 4). While some of this decrease in R^*_{750} can be attributed to the rougher texture of this unit (and more shadowing), the R^*_{750} of the RAT hole interiors (Table 5) of units B and C are also low. These units represent a zone of diagenetic recrystallization somewhat less well developed than that below the Whatanga contact (the more highly developed zone of recrystallization corresponding to unit E1) [*Grotzinger et al.*, 2005; *McLennan et al.*, 2005].

4.4.2.3. Karatepe Unit D

[40] After unit A, D has the highest R^*_{750}. It has the highest red/blue ratios and, along with unit A, has the greatest spectral inflection at 535 nm (Figure 23) of the undisturbed Karatepe stratigraphic units. The undisturbed unit D surface has a convex NIR spectral shape, but the interior of the unit D RAT hole has a concave NIR spectral shape. Unit D is an example of the "redder" colored outcrop discussed in section 4.1.

4.4.2.4. Unit E1

[41] Unit E was divided into subunits E1 and E2. These subdivisions differ in terms of their R^*_{750} values (E1 is darker) and a number of other significant spectral parameters. In fact, the E2 unit is very similar to the F unit and is discussed with that unit in the following section. The E1 unit was observed to have a coarser texture than higher R^*_{750} units such as D and A. This is illustrated in Figure 11 with pre-RAT MI images of the target locations that would become the RAT holes London (in unit D) and Grindstone (in unit E1). With its rougher texture, unit E1 also appears to capture more basaltic sand which, in combination with shadowing from the rough texture, inevitably contributes to its lower R^*_{750}. Although, with reference to Table 5, the R^*_{750} values of clean surfaces within the Grindstone RAT hole was the third lowest (after that of the unit B and C RAT holes); thus the low R^*_{750} of unit E1 (and of units B and C) is not due solely to rough textures and the trapping of basaltic sand grains. With units B and C, the undisturbed unit E1 surface has a concave NIR spectral shape and a low 482 to 535 nm slope (Figure 22). E1 also has low red/blue ratios and a shallow spectral inflection at 535 nm (Figure 23). The boundary between units D and E1 represents the Whatanga contact defined by *Grotzinger et al.* [2005], and unit E1 is the zone of recrystallization also referenced by *Grotzinger et al.* [2005] and *McLennan et al.* [2005].

4.4.2.5. Units E2, F, and G

[42] Like units A, and D, undisturbed surfaces on units E2, F, and G have convex NIR spectral shapes, steeper 482 to 535 nm and 535 to 601 nm slopes (Figures 21 and 22). However, unlike those units, units E2 and F have shallower 535 nm spectral inflections (on a par with unit C) and also

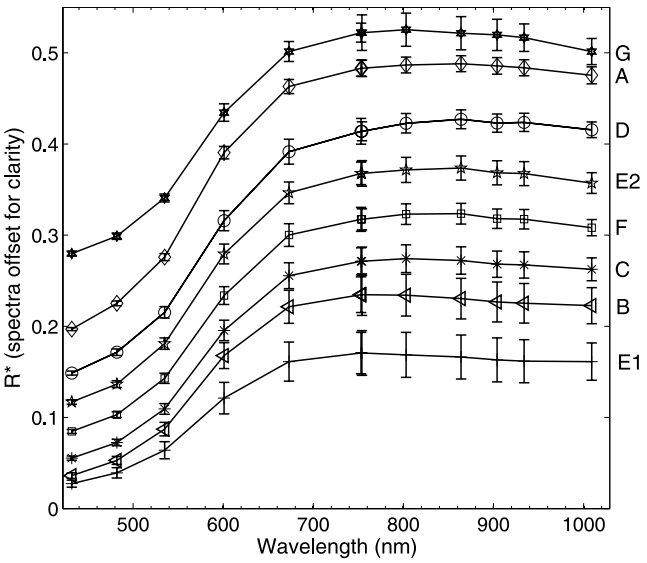

Figure 19. Endurance crater Karatepe ingress stratigraphy spectra. Spectra are offset for clarity but are arranged in approximate order, from top to bottom, from brightest to darkest. Unit C has been offset upward by 0.025, unit F has been offset upward by 0.045, unit E2 has been offset upward by 0.065, unit D has been offset upward by 0.09, unit A has been offset upward by 0.11, and unit G has been offset upward by 0.14.

relatively low red/blue ratios (Figure 23). Unit G has a greater inflection at 535 nm than units E2 and F have. Measurements of clean surfaces from the unit E2 RAT hole, "Kettlestone," the unit F RAT hole, "Millstone" and the unit G RAT hole "Diamond Jenness" have concave NIR spectral shapes.

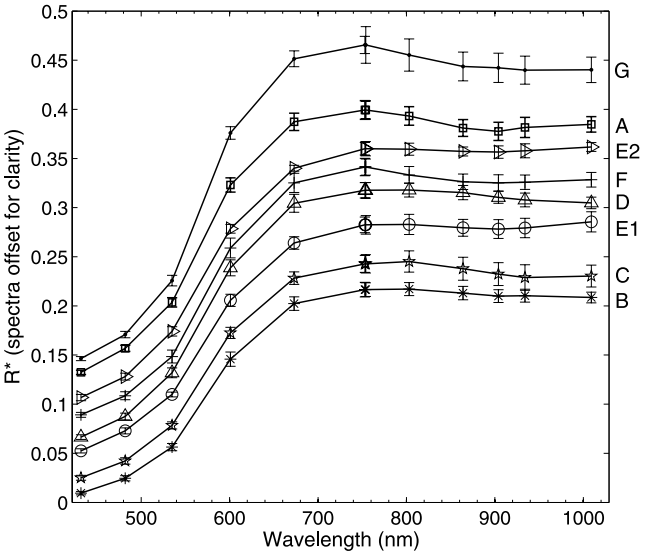

Figure 20. Spectra of RAT-hole interiors of the Karatepe ingress units. A, Tennessee; B, Cobble Hill; C, Virginia; D, London; E1, Grindstone; E2, Kettlestone; F, Millstone; G, Diamond Jenness. B offset down by 0.03, C offset down by 0.02, D offset up by 0.015, F offset up by 0.03, E2 offset up by 0.045, A offset up by 0.06, and G offset up by 0.095.

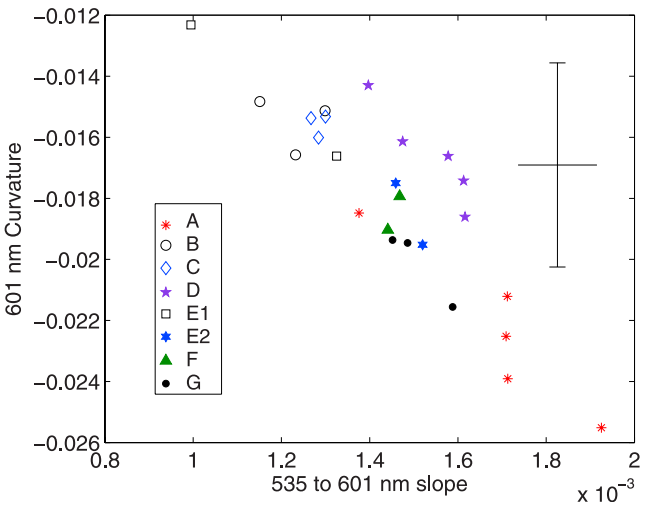

Figure 21. Plot of 601 nm spectral curvature versus 535 to 601 nm slope for Endurance crater, Karatepe ingress region stratigraphic units. Light-toned units are represented by solid and star symbols. Dark-toned units (associated with diagenetic horizons) are represented by open symbols. Error bars, with average standard deviations of these parameters as drawn from unit D measurements, are also shown.

4.5. Outcrop Exposures Observed on the Traverse Toward Victoria Crater

[43] In addition to the outcrop exposures examined at Eagle and Endurance craters, outcrop was observed between those two craters in the Anatolia fracture system, at tiny Fram crater (~5 m diameter), at a number of plains craters

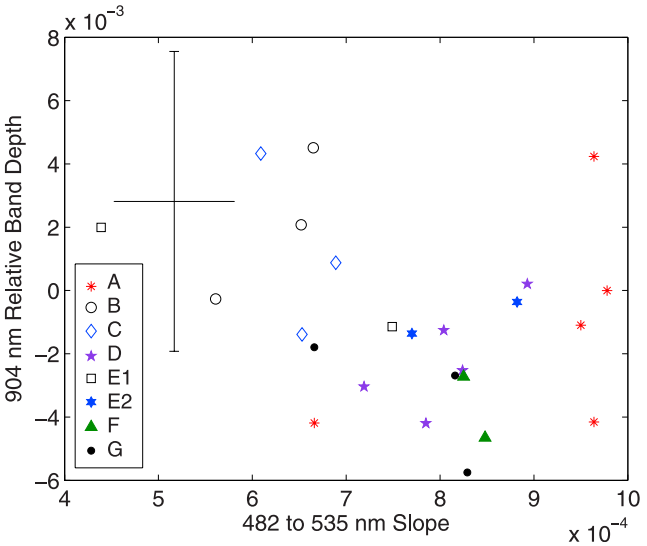

Figure 22. Plot of 482 to 535 nm slope versus 904 nm relative band depth for Endurance crater, Karatepe ingress region stratigraphic units. Error bars, with average standard deviations of these parameters as drawn from unit D measurements, are also shown.

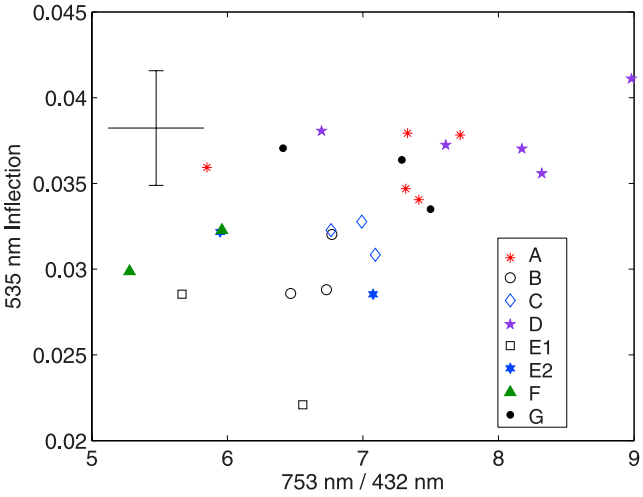

Figure 23. Plot of red/blue (753 nm/432 nm) ratio versus 535 nm spectral inflection for Endurance crater, Karatepe ingress region stratigraphic units. Error bars, with average standard deviations of these parameters as drawn from unit D measurements, are also shown.

south of Endurance (the "southern craters"), and at a number of other locations on the plains. There were more bare exposures of outcrop as Opportunity neared Erebus crater and significant observations were made at the Fruitbasket and Olympia regions (approximately sols 550 to 562 for the former and sols 650 to 740 for the latter). All of these exposures compare closely with those of the Upper Unit of the Burns formation, although hitherto unobserved features such as spherule-free beds in the Olympia outcrop suggest that units encountered in the trek toward Victoria record superjacent stratigraphy, a change in depositional or diagenetic facies, or both. Outcrop along the Anatolia fracture system was not subjected to in situ examination; however, it was observed to have rinds similar in morphology and color to those observed at the Shoemaker's Patio region in Eagle crater (Figures 24a and 24b). Outcrop pavement examined in the Fruitbasket region also had similar rinds (Figure 24c). Representative spectra from Fram crater, southern craters (Viking, and Vostok), southern plains surface exposures ("Fruitbasket"), and from the Olympia outcrop are shown in Figure 25 and spectral parameters from these spectra are shown in Table 6. As with the outcrop at Eagle crater, in L357 composites these additional outcrop exposures display both buff- and purple-colored surfaces (HFS and LFS spectral classes), and have similar NIR characteristics to outcrop at Eagle and Endurance craters.

4.6. Fracture Fill, Rinds, and Cobbles

[44] At Eagle and Endurance craters, and at various locations on the plains, notably at the Fruitbasket and Olympia outcrop regions, materials with distinct color and morphologic properties were observed that have been interpreted variously as coating, rind or fracture fill materials [*McLennan et al.*, 2005]. A more comprehensive discussion of these materials is provided by Knoll et al. (manuscript in preparation, 2007); here we address their VNIR color properties in some detail. These materials fall into three broad classes in terms of their morphology and orientation with respect to bedding: (1) features that are oriented perpendicular, or nearly so, to bedding, (2) those that are oriented coplanar with, or nearly so, to bedding, and (3) those that have random orientations with respect to bedding.

[45] Among the first group are the "Shark Fin" feature in Eagle crater (sol 27), the "Razorback" feature in Endurance crater (sols 162–174), and the "Roosevelt" feature at Olympia (sols 705–725). These materials have been interpreted as fracture fill (Knoll et al., manuscript in preparation, 2007). In the second group are "rinds" at Shoemaker's Patio in Eagle crater (pointed out in Figures 4 and 24a) and "Lemon Rind" and associated features observed in the Fruitbasket region on about sol 556 of Opportunity's mission. The third group is perhaps best exemplified by the "Barbeau" region on the rock "Ellesmere" in Endurance crater (examined around sol 237). Representative spectra from each group are shown in Figure 26. The first and second groups are characterized by moderate to strong inflections at 535 nm and a long wavelength absorption with a band minimum in the 904 nm (R5) band. The third group exhibited more variable spectral properties, although for the portions of the Barbeau region examined, shallower 535 nm band inflections were observed relative to the first two groups. Also, portions of Barbeau exhibited NIR spectral properties similar to the first two groups. Other portions (noted as "coating 2" in Figure 26) had a red slope in the NIR with reflectance in the R7 (1009 nm) band significantly higher than that in the R2 (754 nm) band, similar to the spectra of Meridiani spherules (Figure 7) [*Bell et al.*, 2004; *Weitz et al.*, 2006]. Dark coatings such as those at Barbeau were also observed on the rock Escher examined around sol 208. How the spectral parameters of these rind/fracture fill materials relate to those of other surface

Table 5. Spectral Parameters of RAT-Hole Interiors of the Karatepe Ingress Units[a]

Unit	R^*_{750} ($\times 10^{-1}$)	Red/Blue	482 to 535 nm Slope ($\times 10^{-4}$)	535 nm Inflection ($\times 10^{-2}$)	535 to 601 nm Slope ($\times 10^{-3}$)	601 nm Curvature ($\times 10^{-2}$)	904 nm Relative Band Depth ($\times 10^{-3}$)	754 to 1009 nm Slope ($\times 10^{-5}$)
A	3.32 ± 0.09	4.81 ± 0.14	8.23 ± 0.50	3.97 ± 0.32	1.79 ± 0.08	−3.07 ± 0.45	9.48 ± 6.2	−5.6 ± 2.8
B	2.46 ± 0.07	6.29 ± 0.29	5.91 ± 0.52	2.88 ± 0.41	1.35 ± 0.07	−1.95 ± 0.44	2.06 ± 4.3	−3.4 ± 2.4
C	2.75 ± 0.09	6.12 ± 0.38	7.26 ± 0.61	3.49 ± 0.35	1.49 ± 0.10	−2.34 ± 0.59	1.59 ± 4.7	−5.9 ± 2.8
D	3.02 ± 0.10	6.07 ± 0.33	8.06 ± 0.87	0.748 ± 0.63	1.65 ± 0.11	−2.49 ± 0.54	1.76 ± 4.9	−4.8 ± 2.9
E1	2.79 ± 0.11	6.11 ± 0.66	5.94 ± 0.81	2.53 ± 0.0039	1.16 ± 0.08	−1.44 ± 0.39	1.99 ± 3.8	−5.5 ± 3.3
E2	3.11 ± 0.08	6.51 ± 0.41	8.26 ± 0.72	3.03 ± 0.34	1.49 ± 0.11	−1.85 ± 0.48	6.19 ± 5.0	1.2 ± 2.4
F	3.57 ± 0.08	5.27 ± 0.21	7.18 ± 0.67	4.34 ± 0.41	1.66 ± 0.09	−2.44 ± 0.49	5.08 ± 5.1	−5.8 ± 3.3
G	3.84 ± 0.17	7.39 ± 0.43	11.20 ± 0.73	5.04 ± 0.43	2.33 ± 0.14	−4.32 ± 0.64	4.45 ± 4.0	−12.1 ± 3.4

[a]Values are average values accompanied by standard deviation of the mean.

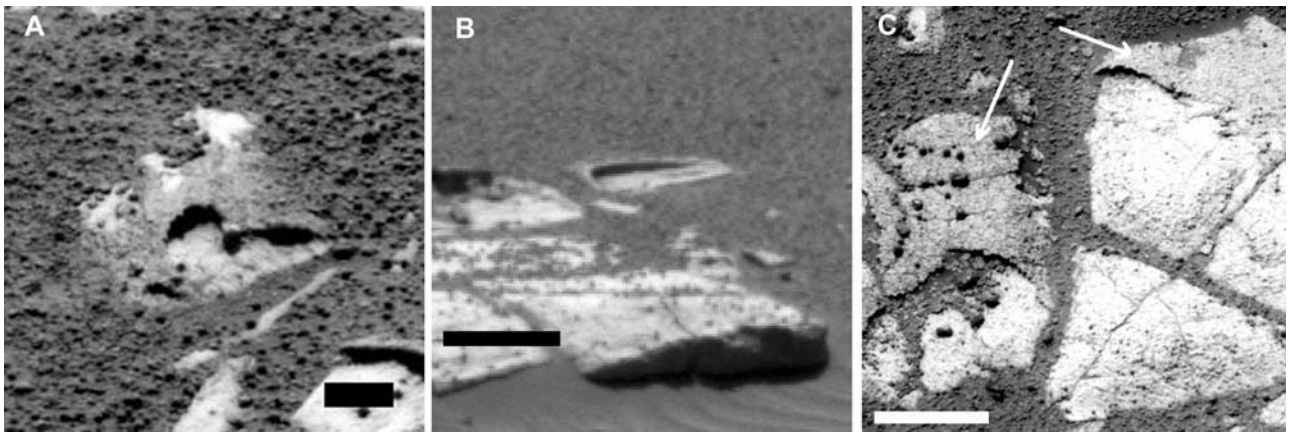

Figure 24. (a) Sol 50 P2579 L3 view of "Golf Hole" rind exposed at Shoemaker's Patio in Eagle crater. Scale bar in bottom right is 4 cm in length. (b) Similar rind over tabular outcrop exposed in the Anatolia fracture system (sol 74 P2591 L3 band). Scale bar in bottom left is 4 cm in length. (c) Similar rinds (marked by arrows) at the Fruitbasket region north of Erebus crater (sol 559 P2586 L3 band). Scale bar in bottom left is 8 cm in length.

materials observed at Meridiani Planum is discussed in section 5.3.

5. Discussion

[46] The trends in the spectral parameter plots of Figures 13–15 and 21–23 provide information regarding the mineralogic character of Meridiani outcrop materials. The multispectral measurements in the VNIR collected by the Pancam can help constrain some of the inferences made by analysis of results from other instruments in Opportunity's Athena science payload [*Squyres et al.*, 2003]. Spectral parameters of the outcrop can also be compared against those of related materials in the Meridiani surface layer (e.g., cobbles, the basaltic sands, and the hematitic spherules).

5.1. Nature of the Meridiani Outcrop

[47] As alluded to in section 4.1, while there are definable differences in the color properties of different stratigraphic horizons in the Burns formation, some of the most fundamental color differences (e.g., the distinction between the HFS and LFS spectral units), may result from weathering effects. One interpretation suggests that many occurrences of the HFS type of outcrop could, in fact, be a weathering rind. We suggest that the HFS veneer comes from extended interactions between outcrop rock surfaces and the atmosphere and/or atmospheric particulates. The HFS veneer might be a result of "acid fog" weathering [e.g., *Banin et al.*, 1997], or could result from interaction of water and airfall dust. In the latter case, dust settles out of the atmosphere, adheres to the surfaces of exposed outcrop, perhaps due to transient films of liquid water and chemical interactions between the dust, outcrop and water produce the HFS veneers.

[48] Despite the common appearance of HFS surfaces, there have been many observations of rocks that seem to lack any evidence of a HFS veneer. We have already noted the rocks Shark's Tooth from Eagle crater and Lion Stone, from the rim of Endurance crater. These rocks appeared to

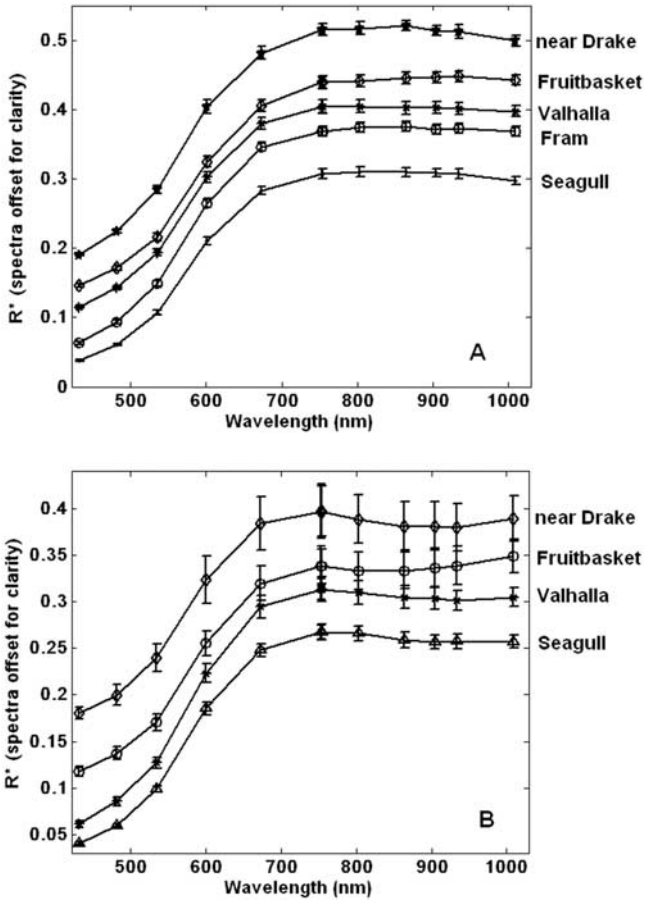

Figure 25. Representative spectra from outcrop other than Eagle and Endurance craters. Spectra (except for the Vostok crater "Seagull" spectrum) are offset for clarity. (a) HFS surfaces. Valhalla (from Viking crater) was offset upward by 0.1, the Fruitbasket area spectrum was offset upward by 0.14, and the "Drake" spectrum (from the Olympia region) was offset upward by 0.18. (b) LFS surfaces. The Fruitbasket area spectrum was offset upward by 0.07. Drake area spectrum was offset upward by 0.11.

Table 6. Spectral Parameters of Outcrop From Fram Crater and From Southern Craters and Plains[a]

Unit	R^*_{750} ($\times 10^{-1}$)	Red/Blue	482 to 535 nm Slope ($\times 10^{-4}$)	535 nm Inflection ($\times 10^{-2}$)	535 to 601 nm Slope ($\times 10^{-3}$)	601 nm Curvature ($\times 10^{-2}$)	904 nm Relative Band Depth ($\times 10^{-3}$)	754 to 1009 nm Slope ($\times 10^{-5}$)
Sol 85 P2532 Fram HFS	3.72 ± 0.08	6.37 ± 0.25	9.89 ± 0.70	4.15 ± 0.31	1.81 ± 0.81	−2.09 ± 0.53	2.25 ± 5.3	4.6 ± 2.7
Sol 403 P2573 Seagull HFS	3.31 ± 0.09	7.45 ± 0.42	9.93 ± 0.51	3.43 ± 0.35	1.66 ± 0.66	−2.08 ± 0.40	−3.29 ± 5.5	−4.90 ± 2.9
Sol 403 P2573 Seagull LFS	2.72 ± 0.12	6.46 ± 0.22	6.86 ± 0.45	3.70 ± 0.35	1.37 ± 0.93	−1.45 ± 0.39	8.54 ± 4.3	−2.10 ± 2.8
Sol 423 P2586 Valhalla HFS	3.64 ± 0.05	6.44 ± 0.36	10.24 ± 0.59	3.55 ± 0.41	1.75 ± 0.76	−2.24 ± 0.51	−2.26 ± 6.1	−2.10 ± 3.3
Sol 423 P2586 Valhalla LFS	2.42 ± 0.15	5.18 ± 0.27	5.18 ± 1.0	3.58 ± 0.55	1.21 ± 0.94	−1.27 ± 0.51	5.51 ± 6.7	−4.00 ± 3.3
Sol 553 P2582 LFS	3.59 ± 0.13	4.78 ± 0.19	8.00 ± 0.76	3.99 ± 0.36	1.57 ± 0.97	−1.59 ± 0.49	2.22 ± 4.6	−4.30 ± 2.6
Sol 561 P2591 Fruitbasket HFS	3.62 ± 0.07	6.37 ± 0.41	8.25 ± 0.91	4.57 ± 0.45	1.74 ± 0.75	−1.90 ± 0.58	−3.89 ± 6.8	1.70 ± 3.4

[a]The "Seagull" target was at Vostok crater; the "Valhalla" target was at Viking crater; and the sol 553 and 561 measurements were both at the "Fruitbasket" region. The Fruitbasket region and Vostok and Viking craters are all marked in Figure 1b.

be displaced and the lack of a weathering veneer could potentially be connected to the time of the formation of the HFS veneer and the time of displacement of those rocks. However, there are also large rocks with LFS surfaces which are seemingly in situ, but are surrounded by rocks with HFS surfaces. It is harder to attribute the lack of a veneer to eolian abrasion in such instances. An example from the Olympia outcrop, the rock "Bellemont," which has a lower 482 to 535 nm slope (LFS class), is shown in Figure 27. Mini-TES observations of such LFS surfaces show that they have a discernable coarse-grained hematite spectral signature, while this signature is weaker to absent in the HFS surfaces (Figure 28). Whether this difference is actually due to higher amounts of coarse-grained hematite throughout the LFS portions of outcrop or just due to the lack of this material in HFS coatings that are thicker than the typical Mini-TES photon penetration depth (50 to 100 μm) is not known.

[49] The view that some observed color differences reflect surficial weathering does not necessarily diminish the value of these surfaces for stratigraphic correlations, as the chemistry of weathering surfaces can still reflect the underlying outcrop composition. We contend that the spectral parameter plots of Figures 13–15 and 21–23 show discernable differences among various HFS-like units. Also, there are subtle differences in the color of fresh outcrop that can be observed in spectra of RAT-hole interiors (Figures 16b and 20; note difference in the NIR slope of

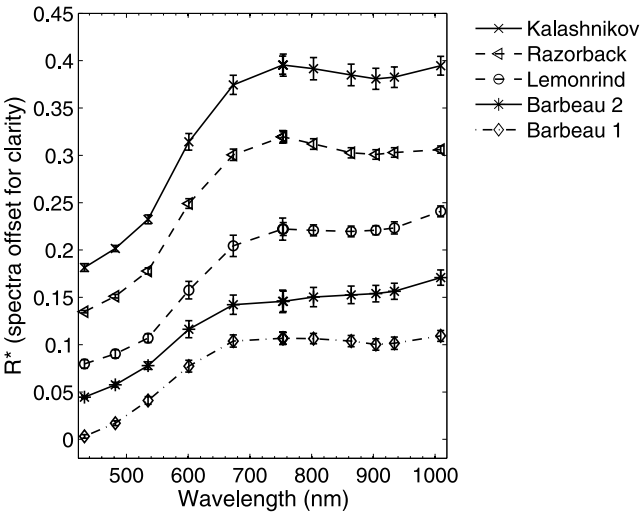

Figure 26. Spectra of coating/fracture fill materials from Eagle and Endurance craters and from the Fruitbasket region. The sol 237 P2588 Barbeau 1 material spectrum was offset downward by 0.02; sol 561 Lemonrind was offset upward by 0.02; sol 175 Razorback was offset upward by 0.045; and sol 50 Kalashnikov was offset upward by 0.06.

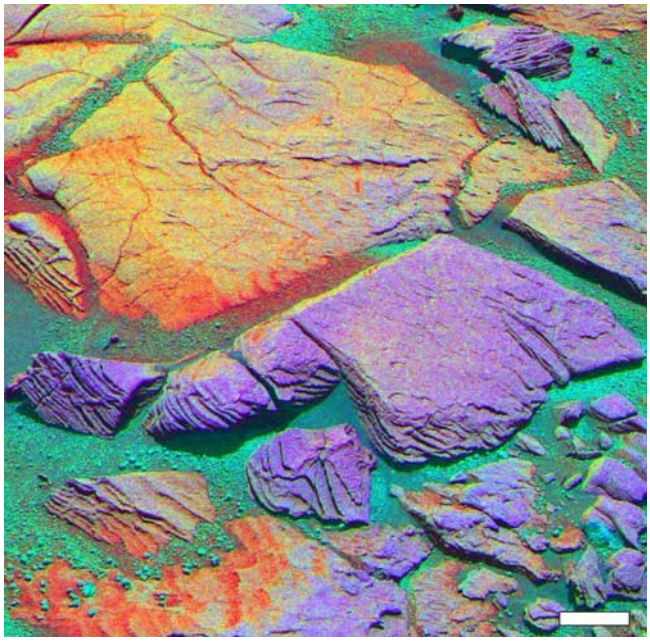

Figure 27. DCS version of band L357 composite of the sol 674 P2541 view of the rock Bellemont at the Olympia outcrop. Note that purple-colored, LFS spectral class, rock, seemingly in situ is adjacent to also seemingly in situ buff-colored HFS surfaced rocks. Scale bar in bottom right is 6 cm long.

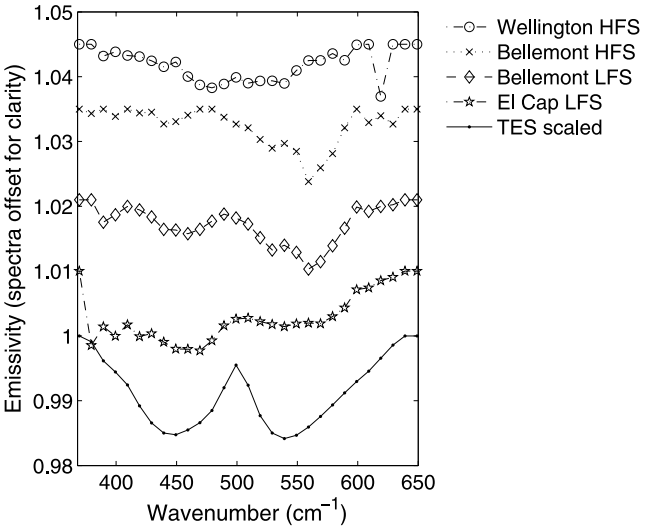

Figure 28. Mini-TES emissivity spectra over HFS and LFS surfaces compared with an orbital TES library spectrum of a hematite-rich surface. Spectra are subsectioned over the 369 to 650 cm^{-1} wave number range and had a straight line continuum removed. LFS surfaces from El Capitan (in Eagle crater) and Bellemont (Olympia region, Erebus crater) display hematite bands centered at 450 and 540 cm^{-1}.

these spectra and the presence or absence of a NIR absorption) and on surfaces that are taken to be relatively unweathered (e.g., the color differences in individual layers in rocks such as Slickrock (Figure 8) and Raspberry Newton (Figure 9)). Accepting these inherent color differences and the mineralogic differences between the HFS and LFS spectral classes observed by the Mini-TES (Figure 28), we should expect that the weathering rinds developed upon them would also have subtle color variations that can be used to support stratigraphic correlations (section 6).

5.2. Comparison of Outcrop Spectra to Known Minerals

[50] In Figure 29, a group of representative Meridiani outcrop spectra are plotted with a group of laboratory measurements of Fe^{3+}–bearing mineral samples reported on and described by *Morris et al.* [2000] (specifically, the sample spectra used are those listed in Table 1 of *Morris et al.* [2000]). The Meridiani outcrop measurements do not fall exclusively within any one field of Fe^{3+}–bearing minerals in either of these spectral parameter plots. In the 482 to 535 nm slope versus 601 nm curvature plot of Figure 29a, the Meridiani outcrop measurements plot along the same trend as, but at an intermediate 601 nm spectral curvature compared to the ferrihydrite and goethite samples. In the 535 to 601 nm slope versus 535 nm spectral inflection plot of Figure 29b, they again plot in-between part of the ferrihydrite and part of the goethite fields. In both spectral parameter plots, some maghemite and schwertmannite samples also plot near the field of Meridiani outcrop measurements and in the 535 to 601 nm slope versus 535 nm inflection plot (Figure 29b), some hematite measurements plot along with ferrihydrite near the Meridiani outcrop measurements. Mineral measurements that consistently plot away from the Meridiani outcrop measurements are lepidocrocite, akaganeite, jarosite, and "goethite 1" (the "goethite 1" samples are the well-crystalline synthetic goethites GTS-2, GTS-3, and GTS-5 reported on by *Morris et al.* [1985]; the "goethite 2" samples, which more closely resemble the Meridiani measurements in the spectral parameter plots, are natural goethites in various stages of crystalline development from nanophase to moderately well crystalline and were discussed by *Morris et al.* [2000]).

[51] Select Meridiani spectra from the Guadalupe and Cathedral Dome features in Eagle crater and from the Emil Nolde dark rind feature on the rock Escher in Endurance crater are plotted in Figure 30a in a continuum-removed and stacked format. These can be directly compared against select library spectra from the *Morris et al.* [2000] suite of samples which are plotted in the same continuum-removed and stacked format in Figure 30b. It can be seen that the Guadalupe RAT hole interior spectrum and the Cathedral Dome LFS surface spectrum have spectral features similar to that of the red hematite spectrum in Figure 30b; i.e., they share a short wavelength absorption with the 535 nm band lower in reflectance than the 482 nm band and a broad long wavelength absorption centered in the 864 to 904 nm range (the pure hematite spectrum has a band center at 864 nm, the Meridiani spectra have this band center offset to 904 nm indicating the presence of other materials besides hematite). The Guadalupe and Cathedral Dome HFS surface spectra lack a well-defined long wavelength absorption and the short wavelength absorption is centered either co-equally between the 482 and 535 nm bands or with the 482 nm band with somewhat lower reflectance. When compared against the library spectra, this could indicate more influence from another phase such as poorly crystalline goethite or schwertmannite (which also have lower reflectance in the 482 vis-à-vis the 535 nm band).

[52] Mössbauer spectrometer measurements indicate the presence of hematite, jarosite, nanophase ferric oxides and an undetermined mineral doublet in the Mössbauer spectra (dubbed the "Fe3D3" phase, it is distinct from the nanophase ferric oxides) [*Klingelhöfer et al.*, 2004]. Given the Mössbauer evidence for jarosite in the Meridiani outcrop, the separation of the field of outcrop measurements from the jarosite field in the spectral parameter plots in Figure 29 requires some examination. As the two known Fe^{3+}–bearing minerals in Meridiani outcrop are hematite and jarosite, a limited set of physical mixtures of jarosite (collected by the first author from Leadville, Colorado) and red hematite powder (sample HMS3 described by *Morris et al.* [2000]) were made. The jarosite was sieved at 150 μm and the less than 150 μm fraction was mixed with the fine-grained (approximately 120 nm particle size) HMS3 hematite. Reflectances of the mixtures were measured by one of us (R.V. Morris) on a Cary 14 spectrophotometer described by *Morris et al.* [2000].

[53] Spectra of these measurements, convolved to Pancam band passes, are shown in Figure 31a and continuum-removed versions of these spectra are shown in Figure 31b. Note that only small admixtures of hematite, on the order of 1%, strongly influence the spectra (consistent with the pigmenting nature of this ferric oxide [e.g., *Morris et al.*, 1985, 1989]). Nevertheless, with increasingly small amounts of hematite, at and less than 0.5%, the center of

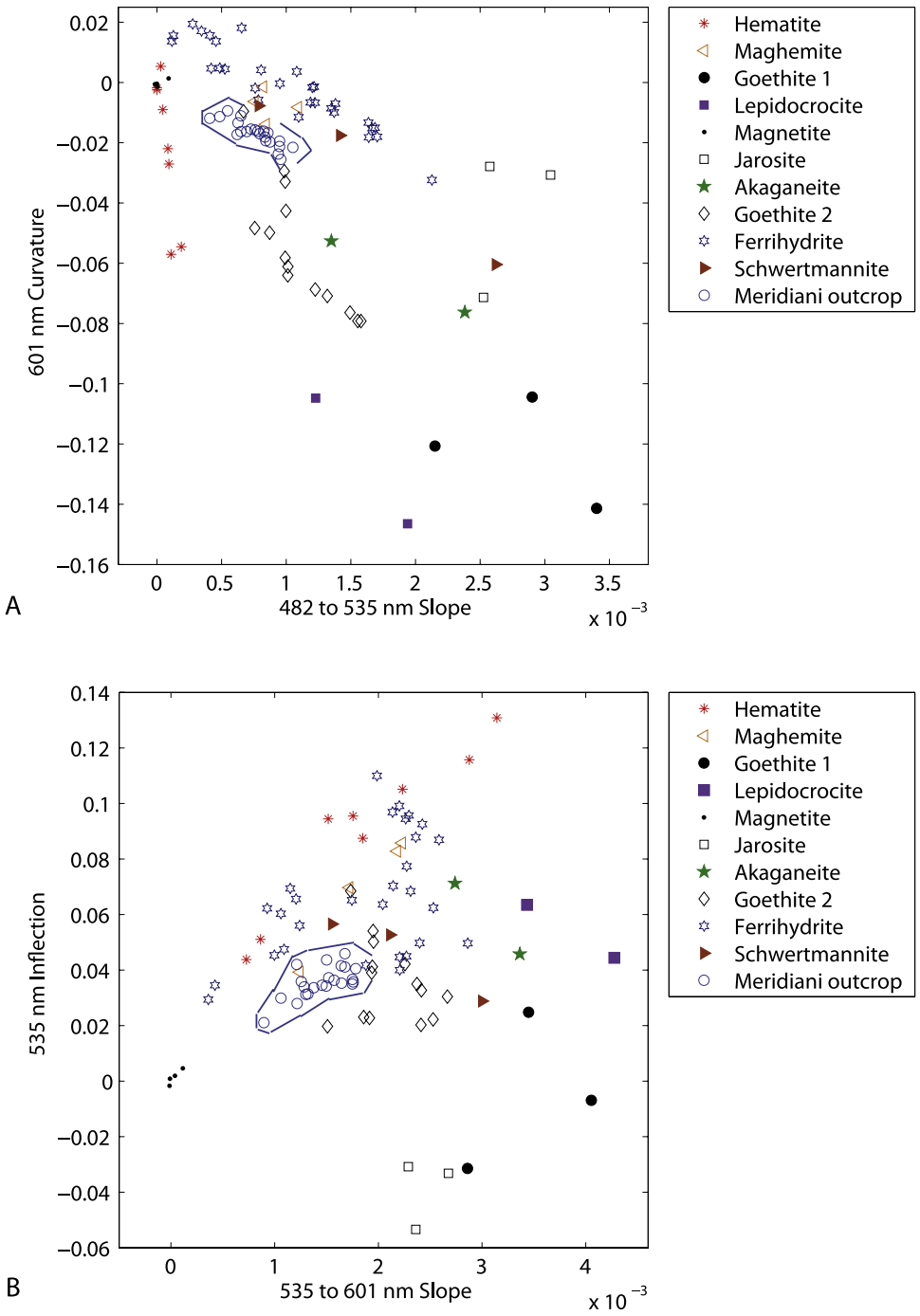

Figure 29. (a) Plot of 482 to 535 nm slope versus 601 nm spectral curvature for laboratory measurements of ferric oxide mineral species and Meridiani outcrop measurements (the overall group of open circles representing the Meridiani outcrop is circled). (b) Plot of 535 to 601 nm slope versus 535 nm spectral inflection for laboratory measurements of ferric oxide mineral species and the Meridiani outcrop measurements.

the long wavelength absorption in the spectra in Figure 31a shifts from the 864 nm band center to the 904 nm band center. In the continuum-removed spectra of Figure 31b, with amounts of hematite less than 0.25%, the short wavelength band center shifts from the 535 nm band center to the 482 nm band center. In a spectral parameter plot of 535 nm spectral inflection versus 535 to 601 nm slope showing just hematite, jarosite and the hematite/jarosite mixtures (Figure 32), the mixture measurements form a trend extending from the hematite field to the jarosite field.

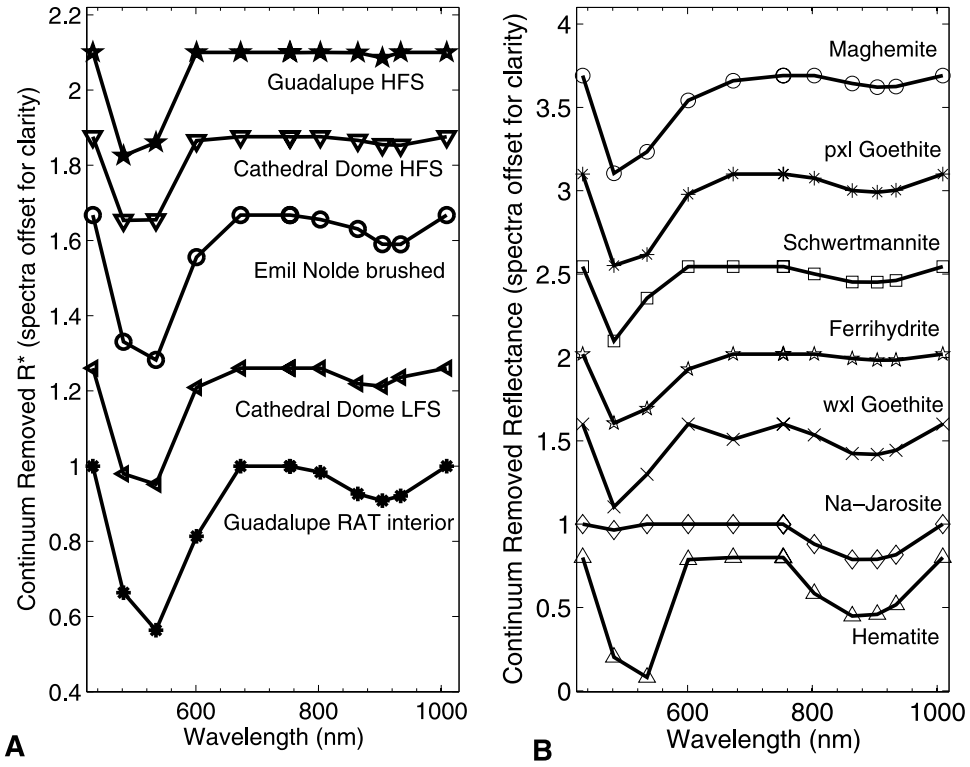

Figure 30. (a) A select group of spectra of surfaces from within Eagle crater and a RAT-brushed dark rind (the "Emil Nolde" feature) from the rock Escher in Endurance crater presented in a continuum-removed and stacked format. (b) A select group of the library spectra described by *Morris et al.* [2000] convolved to Pancam band passes and presented in the same continuum-removed and stacked format. These spectra include poorly crystalline ("pxl") and well-crystalline ("wxl") goethite.

Representative Meridiani outcrop measurements are also plotted in Figure 32. The fact that the field of Meridiani outcrop measurements plots closer to the hematite field potentially indicates that the strong pigmenting effect of hematite overwhelms the spectral features of jarosite. The fact that in Figure 29, the Meridiani outcrop measurements also plotted close to the ferrihydrite and "goethite 2" fields (and some schwertmannite and maghemite measurements) could indicate that one or more of these phases are also present as the unidentified "Fe3D3" phase detected in Mössbauer spectrometer measurements [e.g., *Klingelhöfer et al.*, 2004]. Mössbauer spectra are inconsistent with the hypothesis that maghemite or well-crystalline goethite is the Fe3D3 phase; however, the Mössbauer spectrometer measurements would allow for nanophase goethite as being the Fe3D3 phase [*Klingelhöfer et al.*, 2004; *Morris et al.*, 2006]. Indeed in Figure 29, the Meridiani outcrop field of measurements plot closer to the "goethites 2" field, which includes nanophase goethites, than to the "goethites 1" field, which consists of well-crystalline goethites. Alternatively, the possibility that schwertmannite is the Fe3D3 phase would also be allowed by the Mössbauer spectrometer measurements. *Bishop and Murad* [1996] and *Tosca and McLennan* [2006] have noted that one of the minerals most likely to form from the breakdown of basaltic precursor material with the addition of sulfur is the mineral schwertmannite.

5.3. Spectral Parameters of Outcrop Compared to Other Surface Materials

[54] The basaltic sand, hematite-rich spherules, and sulfate-rich outcrop of Meridiani Planum are distinct chemically, and examination of the VNIR spectral parameters of these materials indicates interesting trends between them. Figure 33 shows a plot of 535 to 601 nm slope versus 535 nm inflection for basaltic sand, hematite spherules, and different color units within Unit A of Eagle crater (the Shoemaker's Patio region). There is a clear trend of increasing 535 to 601 nm slope and greater inflection at 535 nm from the spherules to the basaltic sand to the rinds and then a split between the LFS and HFS surfaces of Unit A. A similar trend is observed in a plot of 535 nm spectral inflection versus 601 nm spectral curvature among comparable surface materials from the Fruitbasket and Olympia regions (Figure 34). These plots illustrate that the Meridiani spherules, both those dislodged from but near the outcrop and loose in the surface layer, are dominated by gray, rather than red, hematite because they have the shallowest 535 nm band inflections and lowest 535 to 601 nm slope of any of the surface layer materials. They also indicate that basaltic sand has slightly higher values for

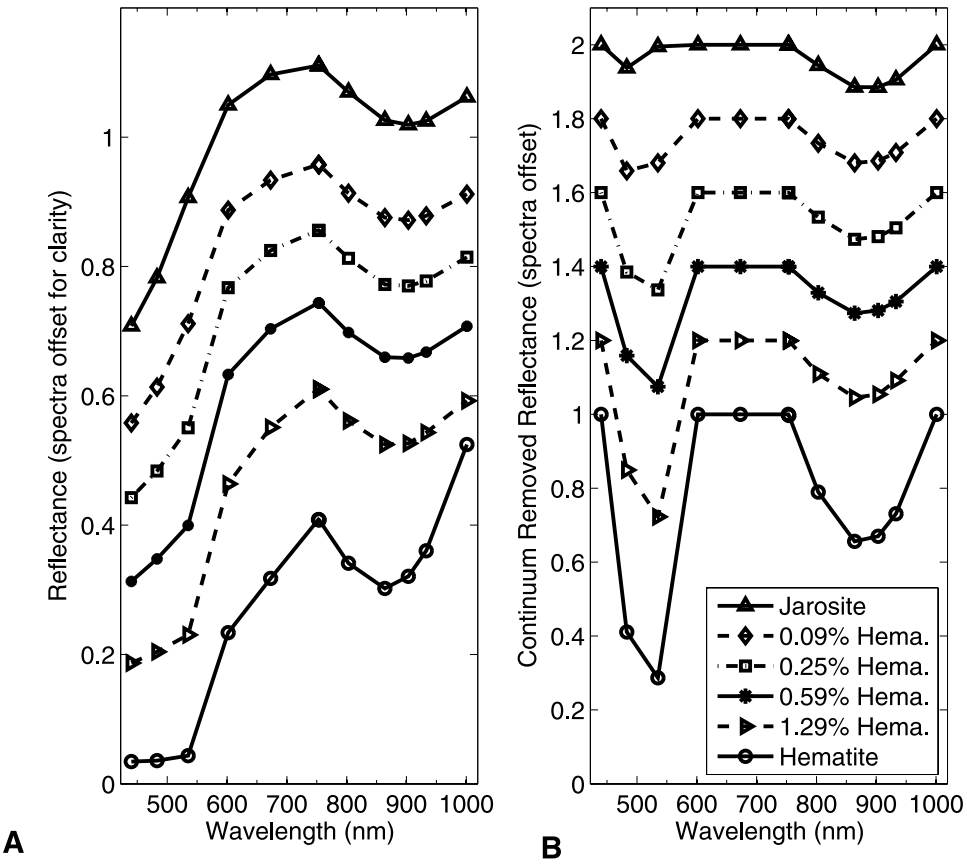

Figure 31. (a) Laboratory reflectance measurements of physical mixtures of hematite and jarosite powders convolved to Pancam band passes. (b) Continuum-removed versions of the spectra shown in Figure 31a.

these parameters, which could indicate minor amounts of oxidation in some of the component materials of the sand and/or inclusion of some component of the highly oxidized windblown bright drift material (dust).

[55] The rinds and fracture fills have higher values for these parameters, but are still lower than those of the outcrop, suggesting material with an overall oxidation level between that of the outcrop and that of the ferrous-mineral-dominated basaltic sand. This is consistent with in situ observations of the "Lemon Rind" target around sol 560 in which the APXS found higher values of the highly mobile elements Na and Cl in the rinds relative to the outcrop [*Yen et al.*, 2006]. The formation mechanism(s) for the rinds and fracture fill is/are still to be determined (the two features could have different origins). Possibilities for the origin of the rind and fracture fill material range from physical mixtures (e.g., something akin to clastic dikes) to in situ alteration of outcrop by diagenetic fluids or atmospheric constituents (Knoll et al., manuscript in preparation, 2007). *Squyres et al.* [2006b] suggest that the rinds observed at the Shoemaker's Patio and Fruitbasket regions might form as form as a result of chemical interactions with the atmosphere when outcrop is close to the atmosphere but is protected from eolian erosion by a thin cover of soil.

[56] The cobbles observed by Opportunity are discussed by *Jolliff et al.* [2006]; however, to summarize, there appear to be at least three groups of cobbles. First, among these are rocks interpreted as meteorites: the cobble examined in situ outside of Endurance crater on sol 123, Barberton, has been interpreted as a meteorite [*Jolliff et al.*, 2006; C. Schröder et al., Meteorites on Meridiani Planum, manuscript in preparation, 2007] and, though larger than a cobble, Heat Shield rock, examined on and around sol 340 is an Fe-Ni meteorite [*Morris et al.*, 2006]. Second, there are cobbles and displaced larger rocks that appear to be crater ejecta. Bounce rock, examined during sols 59–68, was determined to have a chemical composition similar to the SNC meteorite EETA79001 [*Rieder et al.*, 2004]. Likewise, the rocks Lion Stone (examined on and around sol 106) and Russet (examined on and around sol 381) have the composition typical of Meridiani outcrop and have been interpreted as outcrop displaced by impact processes [*Jolliff et al.*, 2006]. The third group is more enigmatic and has been described as the "Erebus clan" by *Jolliff et al.* [2006] and includes cobbles examined in situ: Perseverance, Arkansas, and Antistasi to the north of Erebus crater. Unnamed examples from this latter group of cobbles are plotted in Figure 34 and it can be seen that these materials have among the shallow-

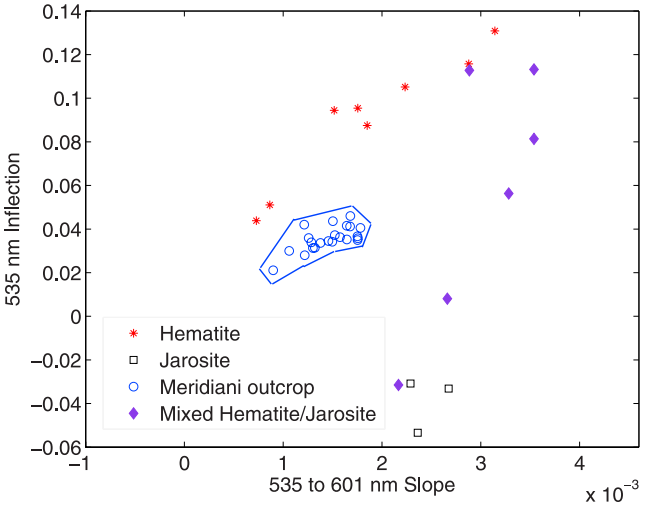

Figure 32. Plot of 535 to 601 nm slope versus 535 nm inflection for *Morris et al.* [2000] measurements of hematite and jarosite samples, physical mixtures of hematite and jarosite, and the representative Meridiani samples from Figure 29.

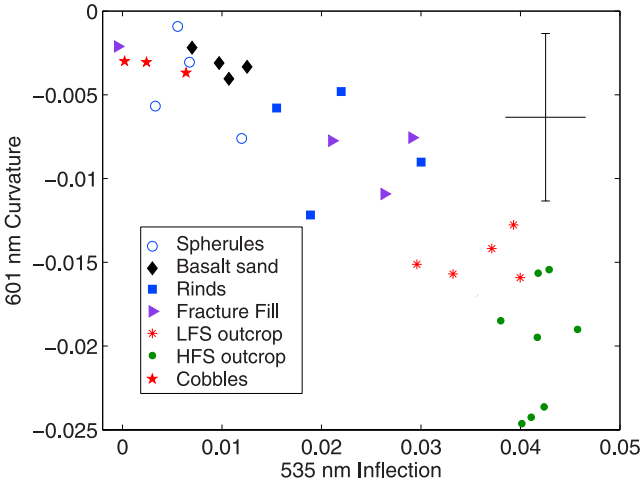

Figure 34. Plot of 535 nm band depth versus 601 nm band depth of surface materials from the Fruitbasket and Olympia regions. Average standard deviations of HFS outcrop measurements are shown as the randomly placed error cross in the top right.

est inflections at 535 nm and shallowest 601 nm curvatures of any of the Meridiani surface materials.

6. Spectral Stratigraphy in Meridiani Planum

6.1. Definition of Units

[57] Early discrimination of units within Eagle crater was based on texture and color [*Squyres et al.*, 2004]. The color information used in these efforts was primarily from L256 composites with manual delineations of boundaries. DCS composites of L256 and L357 composites were also used to help exaggerate color differences. Likewise in Endurance crater, the aforementioned three color composites and DCS variants thereof were used to separate units as is shown in Figures 17 and 35. Interesting color variations were also observed in the Olympia outcrop (Figure 27) and among other outcrop exposures. By incorporating more sophisticated multispectral analyses beyond simple three color composites, our approach on Mars approximates terrestrial studies in "spectral stratigraphy" [*Lang et al.*, 1987; *Lang and Paylor*, 1994].

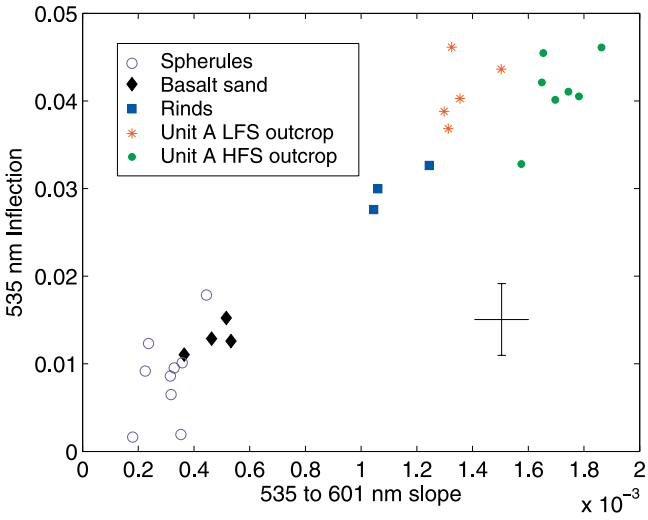

Figure 33. Plot of 535 to 601 nm slope versus 535 nm inflection of surface materials in the Shoemaker's Patio area of Eagle crater. Average standard deviations of HFS outcrop measurements are shown as the randomly placed error cross in the bottom right.

[58] While a R521 composite, such as that in Figure 18, is best suited for highlighting differences between the Endurance crater upper and middle/lower units, observations in the left eye, such as a L357 composite are optimal for distinguishing between component upper unit layers as expressed along the Karatepe ingress path. This is illustrated in the simple three color composite in Figure 17 and the DCS composites in Figure 35.

6.2. Relating Near-Field Unit Observations to Distant Observations

[59] A good correspondence was noted between spectra of stratigraphic units obtained in situ along the Karatepe ingress path and those of the same units observed remotely from pan position 1. Examination of these units as correlated around the crater walls [*Grotzinger et al.*, 2005] indicates that the B and C units pinch out in places and, at least in terms of discussions of remote observations of the stratigraphy are best discussed as a single unit. The units that are most prominent, as observed remotely around the inner crater wall, are the A, B/C, D, and E1 units and these, along with the partially covered by sand and spherules E2 through G units, are summarized in the stratigraphy graphic in Figure 10.

[60] In trying to relate the in situ/near-field observations of Endurance crater stratigraphy to more distant parts of the outcrop, two types of comparisons can be made. First, there are actual remote/far-field observations such as those collected from the rim of Endurance crater at the two "pan positions." Second, there are near-field observations of the

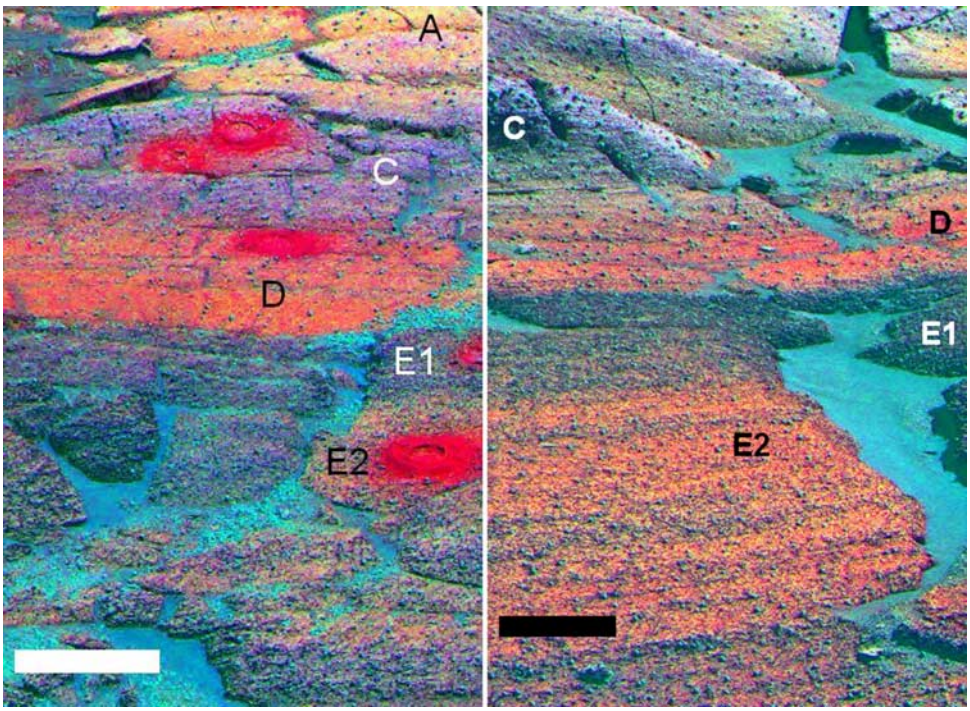

Figure 35. Comparison of the stratigraphic sections (left) at Karatepe West and (right) at Burns Cliff. The image on the left is a subsection from the sol 173 P2401 sequence showing a L357 decorrelation stretch. The A, C, D, E1, and E2 units are annotated. In this image, unit B does not appear spectrally distinct from unit C. The image on the right is a subsection from the sol 288 P2446 sequence, again showing a L357 DCS image. Scale bars in both images are 10 cm in length. The C, D, E1, and E2 units are annotated. The A unit was not captured in this image frame. The E2 unit appeared to be more fractured with more associated basalt sands in the Karatepe West region.

outcrop collected by Opportunity on the east side of the Burns cliff outcrop and at the Karatepe ingress and egress routes. In both cases, relating these observations to the near-field observations of the Karatepe ingress stratigraphy is complicated (1) by differences in spatial sampling, (2) by differences in viewing geometries, and (3) possibly by changing skylight illumination influences on inclined surfaces (up to 30°, or more for remote observations of steeper sections of Endurance's inner rim).

[61] A visual correlation, using L357 DCS images, of units observed at Karatepe West and those at Burns Cliff is presented in Figure 35. In this figure, DCS images from both regions are shown with good agreement between the colors of units C, D, and E1 from both regions.

[62] An example of placing new observations into the stratigraphic context determined by earlier observations was provided as Opportunity exited Endurance crater via the Karatepe east route. Here Opportunity examined the Whatanga contact, between a lower, rough textured unit and an upper, smooth textured unit (Figure 36). The smooth-textured unit with spectral characteristics of the HFS color class is referred to here as the Paikea unit after the Paikea RAT hole ground into it. The rough-textured unit, of the LFS spectral class is called the Wharenhui unit after the Wharenhui RAT hole [*Grotzinger et al.*, 2005]. Figure 37 shows the plot of 535 to 601 nm slope versus 601 nm curvature from Figure 21, with measurements of these parameters for the undisturbed Paikea and Wharenhui units

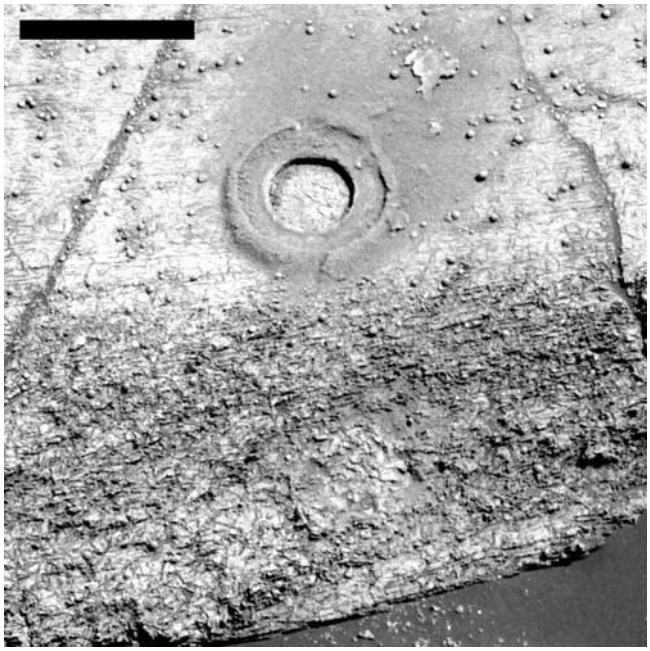

Figure 36. Sol 310 P2558 L3 view of the Paikea (smooth textured, top) and Wharenhui (rough textured, bottom) units referenced in the text. Scale bar in the top left is 10 cm in length.

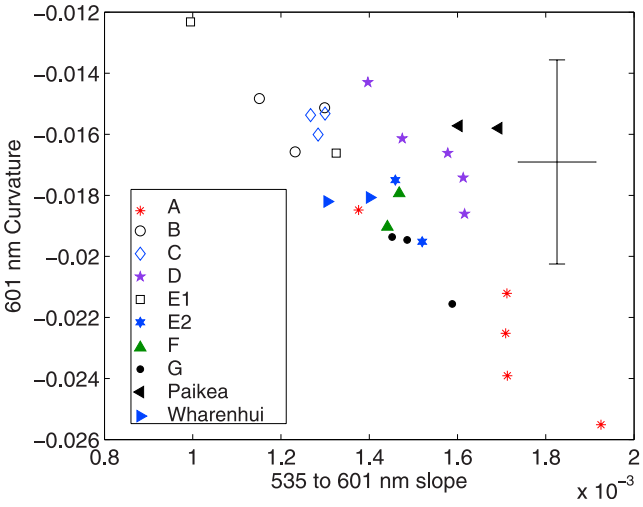

Figure 37. Plot of 535 to 601 nm slope versus 601 nm curvature for Endurance crater Karatepe ingress stratigraphic units with measurements from the Paikea and Wharenhui region overlaid. Representative error bars are included.

also plotted. It can be seen that the Paikea measurements plot closest to the unit D field. The Wharenhui surface measurements plot in an open area near unit E2 and F measurements. Unit E1 measurements, which at the Karatepe ingress path directly underlies unit D, plot further away from the Wharenhui points. However, as discussed above, units B, C and E1 can be seen to pinch out and expand. The boundaries of the E and F units are not so well defined (due, at least in part, to their being partially covered by spherules and basalt sands), but at the Karatepe east egress route, unit E1 very likely might have pinched out leaving E2 adjacent to unit D. The correlation of Paikea and Wharenhui with Karatepe units D and E can also be made on the basis of texture and tone.

[63] Another example, covering a wider gap of both space and time is provided in Figure 38 in which the 535 to 601 nm slope and 601 nm curvature of the sol 561 Fruitbasket measurement are shown on the plot of these parameters for the Eagle crater units. As was noted above, the area that includes the Fruitbasket outcrop has rinds resembling those observed at Shoemaker's Patio in Eagle crater. Morphologic evidence for similarity between the two sets of outcrop is reinforced by spectral evidence in Figure 38 in which the measurements of HFS and LFS spectral units at Fruitbasket plot within the fields of HFS and LFS Eagle unit A outcrop.

7. Summary and Conclusions

[64] Examination of multispectral data collected by Opportunity's Pancam shows that the rock outcrops of the Burns formation examined at Meridiani Planum consist of two main color units which in stretched L357 (673, 535, and 432 nm) composites appear buff-colored and have a **H**igher **F**our hundred eighty-two to 535 nm **S**lope (the **HFS** spectral unit) and purple-colored (with a **L**ower **F**our hundred eighty-two to 535 nm **S**lope, the **LFS** spectral unit). The HFS portions of the outcrops have relatively high 482 to 535 nm and 535 to 601 nm slopes, greater spectral curvature near 601 nm, greater inflections in their spectra near 535 nm and flat to convex NIR spectra. The outcrop surfaces with LFS characteristics tend to have shallower 535 to 601 nm slopes, less curvature in spectral shape near 601 nm, shallower inflections at 535 nm and flat to concave NIR spectra (NIR absorption features centered at 904 nm). These spectral characteristics are consistent with the LFS outcrop consisting of less oxidized, and the HFS outcrop of more oxidized iron-bearing material.

[65] Although the exact nature of these distinct color units has yet to be conclusively determined, it is hypothesized here, and discussed also by Knoll et al. (manuscript in preparation, 2007), that the HFS portions of the outcrop could be a weathering rind caused by the interaction of the outcrop with the atmosphere and/or with atmospheric particulates. It has also been suggested that these veneers could be the residue of a soil-rock weathering interface formed while the outcrop was shallowly buried (R. Sullivan, personal communication, 2006). Nevertheless, there are subtle inherent color variations between different portions of the outcrop (revealed by RAT grinding), and indeed between different weathered HFS surfaces, that have been categorized in this paper. While there are seemingly in situ LFS spectral class rocks surrounded by HFS covered rocks (e.g., the rock Bellemont at the Olympia outcrop, Figure 27) for which the idea of eolian stripping is harder to reconcile, many instances of LFS class surfaces occur on distal faces of layers (Figure 4) and on massive recrystallized portions of the outcrop (Figure 6) which would be most subject to eolian stripping of a HFS veneer. Some of the rocks which appear most devoid of any HFS spectral characteristics appear to be rotated or simply out of place (e.g., the rocks Shark's Tooth (Figure 9) and Lion Stone. If these rocks were displaced, it might be that the formation of the HFS veneer occurred during a specific episode in Mars' climatic history, perhaps during a period of greater orbital obliquity

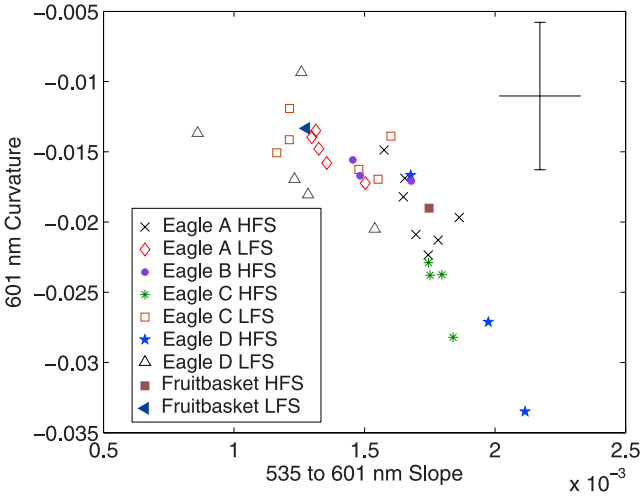

Figure 38. Plot of 535 to 601 nm slope versus 601 nm band depth for Eagle crater units with measurements of the sol 561 measurements of "Fruitbasket" near the Erebus crater "Parking Lot." The "Fruitbasket HFS" and "Fruitbasket LFS" measurements plot with the Eagle A HFS and Eagle A LFS measurements. Representative error bars are included.

[*Mellon and Jakosky*, 1995] when there could have been enhanced condensation at equatorial latitudes. If so, the displacement of rocks such as Lion Stone might postdate that period of weathering. Alternatively, the compositional or mineralogic character of some rocks, perhaps with higher fractions of hematite, might be more resistant to the weathering process that causes the formation of the HFS veneer.

[66] Whereas there was only 30 to 50 cm of stratigraphic section exposed at Eagle crater, a thicker stratigraphic section was examined at Endurance crater. Interpretations by *Grotzinger et al.* [2005] and *McLennan et al.* [2005] have separated this section into an Upper, Middle, and Lower unit with the Middle and Lower unit consisting of beds deposited by eolian activity and the Upper unit consisting of beds deposited by both eolian and aqueous activity with a zone of recrystallization lying between the Upper and Middle units. The middle and lower part of the Upper unit was most extensively examined along the Karatepe West ingress route and consists of primarily HFS units (A and D) with other units (B and C) being more like the LFS spectral class. The E1 unit corresponds to the aforementioned zone of recrystallization with overlap of this zone into the E2 unit with the E1 unit falling into the LFS class and the E2 and underlying F and G units, being in the HFS class.

[67] Exposures of outcrop examined by Opportunity on its southern traverse toward Victoria crater appear to be exclusively of the Upper unit. Examination of spectral parameters, as plotted in Figure 38, indicate that outcrop, for example in the ''Fruitbasket'' area, corresponds to the Eagle unit A; however, we acknowledge that, given the similar chemistry of outcrop layers that this match in spectral parameters is not definitive evidence that these two locations are at the same stratigraphic level.

[68] In addition to the HFS and LFS spectral classes, there are also darker toned rind and fracture fill materials, examined in more detail by Knoll et al. (manuscript in preparation, 2007), and displaced dark-toned cobbles discussed by *Jolliff et al.* [2006]. In this study, we noted that in spectral parameter plots such as Figures 33 and 34, these materials plot between the fields defined by basaltic sands and standard outcrop materials. This suggests, but by no means conclusively demonstrates, that these materials are composed of materials with iron oxidation levels between that of basaltic sands and of the Burns formation outcrop. *Yen et al.* [2006] observed that the rinds are enriched in Na and Cl and might have had halite crystals embedded in them. Some instances of rinds might represent case hardening of outcrop (R. Sullivan, personal communication, 2006). *Squyres et al.* [2006b] suggest that the rinds form as a result of chemical interactions with the atmosphere when outcrop is close to the atmosphere but is protected from eolian erosion by a thin cover of soil, and that the fracture fill materials are composed of intraclastic material derived from adjacent outcrops (discussed also by Knoll et al. (manuscript in preparation, 2007)).

[69] The nature of the Burns formation outcrop is also considered in terms of how spectral parameters derived from multiple measurements compare with laboratory spectra of Fe^{3+}–bearing terrestrial minerals measured by *Morris et al.* [2000]. The Burns formation outcrop plots in a field between goethite and ferrihydrite (Figure 29). Some schwertmannite and maghemite measurements also plot near the Meridiani outcrop field. In spectral parameter plots of just hematite and jarosite, the two Fe^{3+}–bearing minerals known to exist in the outcrop on the basis of Mössbauer spectrometer measurements [*Klingelhöfer et al.*, 2004], outcrop spectral values plot closer to the hematite field (Figure 32). This is consistent with the view that the pigmenting effect of hematite is overwhelming the spectral response of jarosite in the outcrop. The proximity of the Meridiani Planum field of measurements in the spectral parameter plots of Figure 29 to laboratory measurements of schwertmannite and nanophase to poorly crystalline goethite indicates that these minerals (albeit not well-crystalline goethite) are candidates for the Fe3D3 phase identified by the Mössbauer Spectrometer [*Morris et al.*, 2006].

[70] The extensive multispectral observations made by Opportunity, used in conjunction with information from other Athena science payload instruments, have contributed greatly to our understanding of the bedrock exposed at Meridiani Planum. The data also have the potential to be used extensively in the future to aid in regional mapping as high spatial resolution probes of the nature of Meridiani outcrop, when used in conjunction with higher spectral resolution, but lower spatial resolution data from the Mars Express orbiter's OMEGA spectrometer, and from data that will be returned from the Mars Reconnaissance Orbiter (MRO) Compact Reconnaissance Imaging Spectrometer for Mars (CRISM).

[71] **Acknowledgments.** We are grateful to the dedication and professionalism of the entire Athena science team and to the engineers who have made this mission so successful. Funding for Athena science team members was provided by NASA contracts through Cornell and the Jet Propulsion Laboratory. Thanks to Rongxing Li and Yunhang Chen of Ohio State University for Opportunity traverse maps. We are also grateful to helpful reviews by Gregg Swayze and John Mustard.

References

Adams, J. B., M. O. Smith, and P. E. Johnson (1986), Spectral mixture modeling: A new analysis of rock and soil types at the Viking Lander site, *J. Geophys. Res.*, *91*, 8098–8112.

Adams, J. B., M. O. Smith, and A. R. Gillespie (1993), Imaging spectroscopy: Interpretation based on spectral mixture analysis, in *Remote Geochemical Analysis: Elemental and Mineralogical Composition*, edited by C. M. Pieters, and P. A. J. Englert, pp. 145–166, Cambridge Univ. Press, New York.

Arvidson, R. E., et al. (2004), Localization and physical property experiments conducted by Opportunity at Meridiani Planum, *Science*, *306*, 1730–1733.

Banin, A., H. Kan, and A. Cicelsky (1997), Acidic volatiles and the Mars soil, *J. Geophys. Res.*, *102*(E6), 13,341–13,356.

Bell, J. F., III, et al. (2000), Mineralogic and compositional properties of Martian soil and dust: Results from Mars Pathfinder, *J. Geophys. Res.*, *105*, 1721–1755.

Bell, J. F., III, et al. (2003), Mars Exploration Rover Athena Panoramic Camera (Pancam) investigation, *J. Geophys. Res.*, *108*(E12), 8063, doi:10.1029/2003JE002070.

Bell, J. F., III, et al. (2004), Pancam multispectral imaging results from the Opportunity rover at Meridiani Planum, *Science*, *306*, 1703–1709.

Bell, J. F., III, et al. (2005), Large multispectral and albedo panoramas acquired by the Pancam instruments on the Mars Exploration Rovers Spirit and Opportunity, *Lunar Planet. Sci.*, *XXXVI*, Abstract 1337.

Bell, J. F., III, J. Joseph, J. N. Sohl-Dickstein, H. M. Arneson, M. J. Johnson, M. T. Lemmon, and D. Savransky (2006a), In-flight calibration and performance of the Mars Exploration Rover Panoramic Camera (Pancam) instruments, *J. Geophys. Res.*, *111*, E02S03, doi:10.1029/2005JE002444.

Bell, J. F., III, D. Savransky, and M. J. Wolff (2006b), Chromaticity of the Martian sky as observed by the Mars Exploration Rover Pancam instruments, *J. Geophys. Res.*, *111*, E12S05, doi:10.1029/2006JE002687.

Bishop, J. L., and E. Murad (1996), Schwertmannite on Mars? Spectroscopic analyses of schwertmannite, its relationship to other ferric minerals, and its possible presence in the surface materials of Mars, in *Mineral Spectroscopy: A Tribute to Roger G. Burns*, edited by M. D. Dyar, C. McCammon, and M. W. Schaefer, *Spec. Publ. Geochem. Soc.*, *5*, 337–357.

Burns, R. G. (1993), Origin of electronic spectra of minerals in the visible to near infrared region, in *Remote Geochemical Analysis: Elemental and Mineralogical Composition*, edited by C. M. Pieters and P. A. J. Englert, pp. 3–29, Cambridge Univ. Press, New York.

Christensen, P. R., et al. (2004), Mineralogy at Meridiani Planum from the Mini-TES experiment on the Opportunity Rover, *Science*, *306*, 1733–1739.

Clark, B. C., et al. (2005), Chemistry and mineralogy of outcrops at Meridiani Planum, *Earth Planet. Sci. Lett.*, *240*, 73–94.

Clark, R. N., G. A. Swayze, A. Gallagher, T. V. V. King, and W. M. Calvin (1993), The U.S. Geological Survey Digital Spectral Library: Version 1: 0.2 to 3.0 μm, *U. S. Geol. Surv. Open File Rep.*, *93–592*, 1340 pp.

Farrand, W. H., J. F. Bell III, J. R. Johnson, S. W. Squyres, J. Soderblom, and D. W. Ming (2006), Spectral variability among rocks in visible and near-infrared multispectral Pancam data collected at Gusev crater: Examinations using spectral mixture analysis and related techniques, *J. Geophys. Res.*, *111*, E02S15, doi:10.1029/2005JE002495.

Gillespie, A. R., A. B. Kahle, and R. E. Walker (1986), Color enhancement of highly correlated images: 1. Decorrelation and HIS contrast stretches, *Remote Sens. Environ.*, *20*, 209–235.

Goetz, A. F. H., and B. Kindel (1999), Comparison of unmixing results derived from AVIRIS, high and low resolution and HYDICE images at Cuprite, NV, in *Summaries of the Eighth JPL Airborne Earth Science Workshop*, *JPL Publ. 99-17*, edited by R. O. Green, pp. 151–160, Jet Propul. Lab., Pasadena, Calif.

Green, A. A., M. Berman, P. Switzer, and M. D. Craig (1988), A transformation for ordering multispectral data in terms of image quality with implications for noise removal, *IEEE Trans. Geosci. Remote Sens.*, *26*, 65–74.

Grotzinger, J. P., et al. (2005), Stratigraphy, sedimentology and depositional environment of the Burns Formation, Meridiani Planum, Mars, *Earth Planet. Sci. Lett.*, *240*, 11–72.

Herkenhoff, K. E., et al. (2004), Evidence from Opportunity's Microscopic Imager for Water on Meridiani Planum, *Science*, *306*, 1727–1730.

Herkenhoff, K. E., et al. (2006), Overview of Athena Microscopic Imager results, *Lunar Planet. Sci.*, *XXXVII*, Abstract 1816.

Johnson, J. R., et al. (2006), Spectrophotometric properties of materials observed by Pancam on the Mars Exploration Rovers: 1. Spirit, *J. Geophys. Res.*, *111*, E02S14, doi:10.1029/2005JE002494.

Jolliff, B. L., W. H. Farrand, J. R. Johnson, C. Schröder, and C. M. Weitz (2006), Origin of rocks and cobbles on the Meridiani Plains as seen by Opportunity, *Lunar Planet. Sci.*, *XXXVII*, *Abstract 2401*.

Klingelhöfer, G., et al. (2004), Jarosite and hematite at Meridiani Planum from Opportunity's Mössbauer spectrometer, *Science*, *306*, 1740–1745.

Lang, H. R., and E. D. Paylor (1994), Spectral stratigraphy: Remote sensing lithostratigraphic procedures for basin analysis, central Wyoming examples, *Nat. Resour. Res.*, *3*, 25–45.

Lang, H. R., S. L. Adams, J. E. Conel, B. A. McGuffie, E. D. Paylor, and R. E. Walker (1987), Multispectral remote sensing as a stratigraphic and structural tool, Wind River Basin and Big Horn Basin area, Wyoming, *AAPG Bull.*, *71*, 389–402.

McLennan, S. M., et al. (2005), Provenance and diagenesis of the Burns Formation, Meridiani Planum, Mars, *Earth Planet. Sci. Lett.*, *240*, 95–121.

McSween, H. Y., Jr., et al. (1999), Chemical, multispectral and textural constraints on the composition and origin of rocks at the Mars Pathfinder landing site, *J. Geophys. Res.*, *104*, 8679–8716.

Mellon, M. T., and B. M. Jakosky (1995), The distribution and behavior of Martian ground ice during past and present epochs, *J. Geophys. Res.*, *100*, 11,781–11,799.

Morris, R. V., H. V. Lauer Jr., C. A. Lawson, E. K. Gibson Jr., G. A. Nace, and C. Stewart (1985), Spectral and other physiochemical properties of submicron powders of hematite (α-Fe_2O_3), maghemite (γ-Fe_2O_3), magnetite (Fe_3O_4), goethite (α-FeOOH), and lepidocroicite (γ-FeOOH), *J. Geophys. Res.*, *90*, 3126–3144.

Morris, R. V., D. G. Agresti, H. V. Lauer Jr., J. A. Newcomb, T. D. Shelfer, and A. V. Murali (1989), Evidence for pigmentary hematite on Mars based on optical, magnetic, and Mössbauer studies of superparamagnetic (nanocrystalline) hematite, *J. Geophys. Res.*, *94*, 2760–2778.

Morris, R. V., et al. (2000), Mineralogy, composition and alteration of Mars Pathfinder rocks and soils: Evidence from multispectral, elemental, and magnetic data on terrestrial analogue, SNC meteorite, and Pathfinder samples, *J. Geophys. Res.*, *105*, 1757–1818.

Morris, R. V., J. F. Bell III, W. H. Farrand, and M. J. Wolff (2002), Constraints on Martian global surface mineralogical composition, albedo and thermal inertia from Hubble Space Telescope extended-visible multispectral data, *Lunar Planet. Sci.*, *XXXIII*, Abstract 1913.

Morris, R. V., et al. (2006), Mössbauer mineralogy of rock, soil, and dust at Meridiani Planum, Mars: Opportunity's journey across sulfate-rich outcrop, basaltic sand and dust, and hematite lag deposits, *J. Geophys. Res.*, *111*, E12S15, doi:10.1029/2006JE002791.

Reid, R. J., et al. (1999), Imager for Mars Pathfinder (IMP) image calibration, *J. Geophys. Res.*, *104*, 8907–8926.

Research Systems, Inc. (2004), Environment for Visualizing Images (ENVI) version 4.1, manual, Boulder, Colo.

Rieder, R., et al. (2004), Chemistry of rocks and soils at Meridiani Planum from the Alpha Particle X-ray Spectrometer, *Science*, *306*, 1746–1749.

Savransky, D., and J. F. Bell III (2004), True color and chromaticity of the Martian surface and sky from Mars Exploration Rover Pancam observations, *Eos Trans. AGU*, *85*(47), Abstract P21A-0197.

Sherman, D. M., R. G. Burns, and V. M. Burns (1982), Spectral characteristics of the iron oxides with application to the Martian bright region mineralogy, *J. Geophys. Res.*, *87*, 10,169–10,180.

Singh, A., and A. Harrison (1985), Standardized principal components, *Int. J. Remote Sens.*, *6*, 883–896.

Soderblom, L. A., et al. (2004), Soils of Eagle crater and Meridiani Planum at the Opportunity rover landing site, *Science*, *306*, 1723–1726.

Sohl-Dickstein, J., J. R. Johnson, W. M. Grundy, E. A. Guinness, T. Graff, M. K. Shepard, R. E. Arvidson, J. F. Bell III, P. R. Christensen, and R. V. Morris (2005), Modeling Visible/Near-Infrared photometric properties of dustfall on a known substrate, *Lunar Planet. Sci.*, *XXXVI*, Abstract 2235.

Squyres, S. W., et al. (2003), Athena Mars rover science investigation, *J. Geophys. Res.*, *108*(E12), 8062, doi:10.1029/2003JE002121.

Squyres, S. W., et al. (2004), In situ evidence for an ancient aqueous environment at Meridiani Planum, Mars, *Science*, *306*, 1709–1714.

Squyres, S. W., et al. (2006a), Overview of the Opportunity Mars Exploration Rover Mission to Meridiani Planum: Eagle Crater to Purgatory Ripple, *J. Geophys. Res.*, *111*, E12S12, doi:10.1029/2006JE002771.

Squyres, S. W., et al. (2006b), Two years at Meridiani Planum: Results from the Opportunity Rover, *Science*, *313*(572), 1403–1407, doi:10.1126/science.1130890.

Thompson, S. D., W. M. Calvin, W. H. Farrand, J. R. Johnson, and J. F. Bell III (2006), Fine scale multispectral features of sedimentary bedrock structures of Meridiani Planum, Mars, *Lunar Planet. Sci.*, *XXXVII*, Abstract 1938.

Tompkins, S., J. F. Mustard, C. M. Pieters, and D. W. Forsyth (1997), Optimization of endmembers for spectral mixture analysis, *Remote Sens. Environ.*, *59*, 472–489.

Tosca, N. J., and S. M. McLennan (2006), Constraints on evaporation processes at Meridiani Planum: Combining theoretical and experimental data, *Lunar Planet Sci.*, *XXXVII*, Abstract 2278.

Weitz, C. M., R. C. Anderson, J. F. Bell III, W. H. Farrand, K. E. Herkenhoff, J. R. Johnson, B. L. Jolliff, R. V. Morris, S. W. Squyres, and R. J. Sullivan (2006), Soil grain analyses at Meridiani Planum, Mars, *J. Geophys. Res.*, *111*, E12S04, doi:10.1029/2005JE002541.

Yen, A. S., J. P. Grotzinger, R. Gellert, B. C. Clark, S. M. McLennan, R. V. Morris, C. Schröder, G. Klingelhöfer, K. E. Herkenhoff, and J. R. Johnson (2006), Evidence for halite at Meridiani Planum, *Lunar Planet. Sci.*, *XXXVII*, Abstract 2128.

J. F. Bell III, J. Soderblom, and S. W. Squyres, Department of Astronomy, Cornell University, 428 Space Sciences Building, Ithaca, NY 14853, USA.

W. M. Calvin and S. D. Thompson, Department of Geological Sciences, University of Nevada, Reno, Reno, NV 89557, USA.

W. H. Farrand, Space Science Institute, Boulder, CO 80301, USA.

J. P. Grotzinger, Division of Geological and Planetary Sciences, California Institute of Technology, Pasadena, CA 91125, USA.

J. R. Johnson, U.S. Geological Survey, 2255 North Gemini Drive, Flagstaff, AZ 86001, USA.

B. L. Jolliff, Department of Earth and Planetary Sciences, Washington University, St. Louis, MO 63130, USA.

A. H. Knoll, Botanical Museum, Harvard University, Cambridge, MA 02138, USA.

S. M. McLennan Department of Geosciences, State University of New York, Stony Brook, NY 11794, USA.

R. V. Morris, NASA Johnson Space Center, Houston, TX 77058, USA.

W. A. Watters, Department of Earth, Atmospheric and Planetary Sciences, Massachusetts Institute of Technology, 77 Massachusetts Avenue, Cambridge, MA 02139, USA.

A. S. Yen, Jet Propulsion Laboratory, California Institute of Technology, Mail Code 183-501, 4800 Oak Grove Drive, Pasadena, CA 91109, USA.